(NASA-TM-81352) THE EFFECT OF THERMAL STRESSES ON THE INTEGRITY OF THREE BUILT-UP AIRCRAFT STRUCTURES (NASA) 60 p
HC A04/MF A01 CSCL 01C

N81-12004

Unclas
G3/05 29286

NASA Technical Memorandum 81352

THE EFFECT OF THERMAL STRESSES ON THE INTEGRITY OF THREE BUILT-UP AIRCRAFT STRUCTURES

Jerald M. Jenkins

November 1980

NASA

NASA Technical Memorandum 81352

THE EFFECT OF THERMAL STRESSES ON THE INTEGRITY OF THREE BUILT-UP AIRCRAFT STRUCTURES

Jerald M. Jenkins
Dryden Flight Research Center
Edwards, California

National Aeronautics and
Space Administration

1980

THE EFFECT OF THERMAL STRESSES ON THE INTEGRITY OF THREE BUILT-UP AIRCRAFT STRUCTURES

Jerald M. Jenkins
Dryden Flight Research Center

INTRODUCTION

The impact of temperature variations on aircraft structures does not constitute an insurmountable obstacle, but more accurately a set of intricate complexities. The need for aircraft with Mach 4.5 to 6.0 capabilities between now and the year 2000 has been detailed in reference 1 in which is presented a complex matrix of potential structural approaches. Previous studies (references 2 through 4) have also resulted in many options concerning the character of the structure. Such factors as fuel storage, engine inlet/nozzle environment, and airframe aerodynamic heating create the temperature gradients and variations that result in thermal stresses (references 5 through 10). Laboratory test data suitable for assessing the prediction methods or concept performance is minimal. This places the designer in a serious dilemma since costly laboratory tests have not occurred and analysis approaches have not been extensively explored either. The analysis need has been recognised (references 11 through 13), however, the extent to which the technology has been developed is as yet unknown.

A previous investigation (reference 14) led to a series of laboratory heating experiments on three structural concepts (references 15 through 17). The same three concepts are the nucleus of this paper. The previous studies of these concepts (references 15 through 17) were primarily directed toward predicting laboratory measured thermal stresses using NASTRAN

(reference 18) as the predictive finite element tool. The primary thrust of this paper is to examine the efficiency, performance, and integrity of these three built-up structural concepts subjected to the same laboratory heating tests. The secondary purpose of this paper is to relate these integrity considerations to additional aspects of thermal stress predicting techniques. Measured thermal stresses are examined with respect to material yield strengths, buckling criteria, structural weight, and geometric locations. Principal thermal stresses are presented and studied from the point of view of uniaxial and biaxial stress assumptions.

SYMBOLS

a	long dimension of the plate, m (in)
b	short dimension of the plate, m (in)
C	clamped edge
D	plate cross-section rigidity, $Eh^3/12(1-\mu^2)$, N-m (lb-in)
E	Young's modulus, N/m^2 (lb/in^2)
h	thickness, m (in)
K	buckling coefficient
N	axial load, MN/m (lb/in)
SS	simply supported
T	temperature, °K (°F)
t	time, minutes
x, y, z	rectangular coordinates
ϵ	normal strain
θ_p	angle to principal stress, degrees
μ	Poisson's ratio
σ	normal stress, MN/m^2 (lb/in^2)

σ_S principal stress, MN/m^2 (lb/in^2)

σ_T thermal stress, MN/m^2 (lb/in^2)

SPECIMEN DESCRIPTION

Frame Concepts

Three distinct fuselage frame (ring) concepts were conceived after the completion of the study of reference 14. A built-up test specimen of each of the three concepts was fabricated to represent a portion of the bottom side of the blended wing-body structure. The specimens included the load carrying skin with integral frame stiffeners. The three specimens are shown as a group in figure 1. The frame structure shown in the background of figure 1 (and in more detail in figure 2) is a truss type frame structure constructed of titanium (6Al-4V). This specimen will be referred to hereafter as Frame A. The middle frame structure, shown in figure 1, is fabricated of stainless steel (Type 301) with the frame formed in a Z-shape. This frame specimen will be referred to as Frame B and it is shown in more detail in figure 3. The frame structure in the foreground of figure 1 has a Z-shaped section constructed of titanium (6Al-4V). This frame specimen has the skin fastened to it which is made of Lockalloy (Be-38Al). The skin is interchangeable between the three frame concepts. The frame concept in the foreground of figure 1 will be designated Frame C and a more detailed picture is shown in figure 4.

Weight Analysis

Structural weights were calculated for the three frame specimens with skins attached. The weight was calculated on the basis of the weight per unit skin area for the specimens. A comparison of the relative weights of the three frames is shown in figure 5. Frame A is clearly the heaviest of the three frames; however, Frame B and Frame C are very close to the same weight per unit skin surface area. Frame B is only 2 percent heavier than frame C. Frame A is 8 percent heavier than Frame B and 10 percent heavier than Frame C. It will be helpful for the reader to retain these percentages while reading the remainder of the paper since considerable additional discussion ensues of a comparative nature.

TEST DESCRIPTION

Test Procedure

An overall pictorial description of the heating experiment conducted on the frame/skin structures is illustrated in figure 6. The mission was derived from one of a research aircraft which includes an air launch from a larger aircraft as was done with past rocket research airplanes (references 19 through 22). The upper left part of figure 6 describes the prelaunch climbout portion of the flight where the research airplane is cold soaked because of long time exposure to high altitude cold. The upper right hand part illustrates the postlaunch time history of the fictitious aircraft on a Mach 6 flight in which aerodynamic heating is experienced. The lower part of the figure depicts the manner in which the condition of prelaunch cool down and the postlaunch aerodynamic heating are simulated on the test structure. Liquid nitrogen is gasified and mixed with air to provide the cold sources for cooling the specimens. The gaseous mixture is blown over and around the specimen to achieve cooling. Overcooling is compensated by using radiant heaters to achieve the precise specimen surface temperature. The postlaunch aerodynamic heating is simulated by using radiant heaters to achieve the prescribed surface temperatures on the skins. Thermocouples located on the surface of the skins of the test structure are used to control the heating environment.

A photograph of a portion of the radiant heater is shown in figure 7. An additional photograph showing the specimen (without) the radiant heater) is presented in figure 8. The ducting which supplies the gaseous nitrogen can be seen in the background.

Instrumentation

The primary measurement objectives of the tests were to record strains and temperatures at key locations. Temperatures were measured using Chromel-Alumel thermocouples at all strain gage locations and this type of sensor was used to control the skin temperatures during the tests. Resistance type strain gages were used to measure the thermal stresses. The gages were oriented primarily along the longitudinal axis of the specimen. A nominal number of equiangular strain gage rosettes were located on the skin surface. The test was conducted in the NASA Dryden Flight Research Center Flight Loads Research Facility (reference 23). The test was conducted using analog heating control equipment and the data was recorded on site with the Flight Loads Research Facility data acquisition system.

A photograph showing part of the instrumentation on the skins is presented in figure 9 for Frame A. A more detailed photograph

is presented in figure 10 where the strain gages, thermocouples, and wiring can be better seen.

STRUCTURAL MODELS

Axial thermal stresses have been calculated using experimentally measured temperatures as the loading inputs to several NASTRAN finite element models. Numerous models and model variations were developed for study in references 15 through 17. This paper will utilize only the two NASTRAN models shown in figure 11.

The NASTRAN model used to represent Frame A was developed for one of the symmetrical quarters of the test structure. The model, which has a surface area of 0.34 square meter (3.68 square feet) and a nominal depth of 0.10 meter (4 inches), was composed of 237 bar, rod, and shear panel elements. Similarly, a symmetrical quarter was modeled for use with Frames B and C. This model (see figure 11) was composed of 183 bar and shear panel elements. Additional information concerning the details of these two models is contained in references 15 through 17. The axial thermal stresses calculated using these NASTRAN models are the basis for comparison with the experimentally measured thermal stresses in the previously reported comparisons.

PRINCIPAL STRESSES

At numerous locations on the skin of the test specimens, equiangular strain rosettes were used so that principal stresses could be identified. Three strain measurements, ε_0, ε_{60}, and ε_{120}, are measured at discrete locations. ε_0 is measured in the direction of the axis of the specimen, while ε_{60} is measured at an angle of 60 degrees to the axis of the specimen, and ε_{120} is measured at an angle of 120 degrees to the axis of the specimen. Formulae are derived in reference 24 for calculating principal stresses, σ_{S_1} and σ_{S_2}, and for calculating the angle to the principal stresses, θ_p. The equations used to calculate the principal stresses are:

$$\sigma_{S_1} = E\left[\frac{\varepsilon_0 + \varepsilon_{60} + \varepsilon_{120}}{3(1-\mu)}\right] + \frac{1}{1+\mu}\sqrt{\left[\varepsilon_0 - \frac{\varepsilon_0 + \varepsilon_{60} + \varepsilon_{120}}{3}\right]^2 + \frac{(\varepsilon_{120} - \varepsilon_{60})^2}{3}} \quad (1)$$

$$\sigma_{S_2} = E\left[\frac{\varepsilon_0 + \varepsilon_{60} + \varepsilon_{120}}{3(1-\mu)}\right] - \frac{1}{1+\mu}\sqrt{\left[\varepsilon_0 - \frac{\varepsilon_0 + \varepsilon_{60} + \varepsilon_{120}}{3}\right]^2 + \frac{(\varepsilon_{120} - \varepsilon_{60})^2}{3}} \quad (2)$$

The angle to the principal stress is:

$$\theta_p = \frac{1}{2}\tan^{-1}\left[\frac{\frac{1}{\sqrt{3}}(\varepsilon_{120} - \varepsilon_{60})}{\varepsilon_0 - \frac{\varepsilon_0 + \varepsilon_{60} + \varepsilon_{120}}{3}}\right] \quad (3)$$

BUCKLING ANALYSIS

The buckling of a skin panel due to thermal stress is a very complex plate buckling problem. The definition of the edge restraint is a prominent problem that is usually present when analyzing an aircraft skin. Obviously the edge restraint lies somewhere between a simply supported case and a clamped situation. Also, in the case of a hot structure, transient and nonuniform temperatures lead to nonuniform values of the elastic modulus which results in difficult nonlinearities. The most complicated

problem results from the characteristic nonuniform edge loading which is manifest in plates subject to thermal stress. Thermal stress distributions are very nonlinear and this does not lead to straightforward analysis. The solution of many of these problems is clearly beyond the intended scope of this paper; however, the reader should certainly be aware of the complexity of the situation.

The buckling strength of the skin panels was estimated using the approach and logic described in the following discussion. The general buckling-stress equation is:

$$\sigma_{cr} = \frac{K\pi^2 E}{12(1 - \mu^2)} \left(\frac{h}{b}\right)^2 = \frac{K\pi^2 D}{hb^2} \qquad (4)$$

also

$$\sigma_{cr} = \frac{(N_x)_{cr}}{h} \qquad (5)$$

The symbol D is the plate cross-section rigidity. The buckling strength of a plate (of the dimensional proportions of the test specimen skin panels) which is compressed in one direction with the loaded edge simply supported and the other edges simply supported can be expressed (ref. 25) as:

$$\sigma_{cr} = 4.15 \frac{\pi^2 D}{hb^2} \qquad (6)$$

The buckling strength of a plate compressed in one direction with the loaded edges simply supported and the other two edges clamped can be expressed (ref. 25) as:

$$\sigma_{cr} = 6.98 \frac{\pi^2 D}{hb^2} \qquad (7)$$

The buckling strength of a plate equally compressed in two directions with all the edges simply supported can be expressed (ref. 26) as:

$$\sigma_{cr} = 2.52 \frac{\pi^2 D}{hb^2} \qquad (8)$$

The buckling strength of a plate equally compressed in two directions with the loaded edges simply supported and the other two edges clamped is deduced from equations (6), (7), and (8):

$$\sigma_{cr} = \frac{6.98}{4.15}(2.52)\frac{\pi^2 D}{hb^2} = 4.24\frac{\pi^2 D}{hb^2} \qquad (9)$$

Equations (6), (7), (8), and (9) are the basis for estimating the buckling strength of the skin panels for the test specimens evaluated in this paper.

The plate cross-section rigidity, D, is defined as:

$$D = \frac{Eh^3}{12(1 - \mu^2)} \qquad (10)$$

However, the elastic modulus, E, is a function of temperature which is a function of geometry and time. Hence:

$$D(T, t, x, y, z) = \frac{E(T, t, x, y, z)\, h^3}{12(1 - \mu^2)} \qquad (11)$$

The development of time histories of the estimated buckling strengths used in this paper account for these variables.

UNIAXIAL AND BIAXIAL STRESS

Thermal stresses calculated with the NASTRAN models are constructed of elements that accommodate only uniaxial stresses. It will be seen later that the stress rosettes located on the skin areas of the specimens indicate the stress situation to be clearly biaxial in nature. Hence, the calculated thermal stresses were based on the simplified version of Hooke's Law:

$$\varepsilon_x = \frac{1}{E}(\sigma_x) \qquad (12)$$

The thermal stresses that were measured on the skins of the test structure were obeying the more generalized version (ref. 27) of Hooke's Law:

$$\varepsilon_x = \frac{1}{E}(\sigma_x - \mu\sigma_y) \qquad (13)$$

Poisson's ratio for the skin material is 0.14. It will be shown in subsequent discussions that $\sigma_x \approx \sigma_y$; hence, equation (13) may be rewritten as:

$$\varepsilon_x = \frac{1}{E}(\sigma_x - .14\sigma_x) = \frac{.86}{E}(\sigma_x) \qquad (14)$$

The inaccuracy in comparing uniaxially calculated thermal stress with measured thermal stresses that are in reality biaxial in nature is the difference between equations (12) and (14) respectively for equal x and y thermal stresses. It is important to note that Poisson's ratio for the skin material is unusually small; hence, the discrepancy in the comparison is not as significant as would be the case for other commonly used metal alloys.

RESULTS AND DISCUSSION

Measured Frame Thermal Stresses

The upper cap area (the area adjacent to the skin) is the part of the frame which experiences the largest temperatures. The remainder of the web (or link in the case of Frame A) and the lower cap remain relatively cool (refs. 15 through 17). The frame part of the test specimens will be viewed from two primary viewpoints: (1) the axial thermal stress at selected locations will be examined and compared to the yield strength of the frame material, and (2) the measured axial thermal stress will be compared to calculated values.

Data are presented in figure 12 for the lower cap and middle areas of the three frames. Data are shown for four different strain gage locations. Time histories of measured axial thermal stress are compared with the yield strength of the material. The variation of the yield strength with time is due to temperature increases which degrade the material strength. Toward the end of the time history, it can be seen that the yield strength at R degrades very little (because very little heating reaches location R) and the yield strength at O begins to change measurably because location O is beginning to heat up.

The largest thermal stresses occur on Frame B in contrast to Frame A which has the smallest stresses. The titanium truss configuration of Frame A is probably the major factor resulting in the small stresses since Frame C has higher stresses and is also made of titanium but of a different shape. Frame B has geometry similar to Frame C; however, the highest stresses are noted in Frame B. This implies that combined factors such as heat conduction, elastic modulus, and thermal expansion drastically alter the thermal stresses.

Time histories of thermal stresses for the upper cap areas are shown in figure 13. The material yield lines decrease significantly because the upper cap area is the hottest part of the frame. It can be seen that the largest thermal stresses occur for Frame B. It can also be seen that as the time (and heating) progress, the thermal stresses and the material yield lines tend to converge. The important feature of this convergence is the fact that the structure has a considerably reduced ability to carry loads.

Predicted Frame Thermal Stresses

Time histories of calculated thermal stresses are presented in figure 14 for all three frames. The measured thermal stresses are also presented for comparison at five locations on the frame structures. The upper cap areas (location N) all indicate a trend in which the measured values are less than the predictions. This deviation may be attributed to the fact that the NASTRAN model only accounted for uniaxial stresses (or extensional stresses), when the measured values are potentially experiencing biaxial stress. If the biaxial stress were assumed to be equal, then the deviations, for instance at time equals four minutes, for all three frames is approximately fifteen percent which might correlate with the development of equation (14) in the Uniaxial and Biaxial Stress Section. The same circumstances could explain the discrepancy of the lower cap if the biaxial stresses were of opposite sign. The general agreement, however, between the measured and predicted thermal stresses is quite good. The trends with time and the distribution of stress correlate well with measured data. The discrepancies that do exist between measured and predicted data most likely could be lessened by modeling refinements.

Measured Skin Thermal Stresses

The skin panels of an aircraft structure are a particularly critical component since both strength and elastic stability (buckling) considerations must be addressed. The elastic stability analysis is usually complicated by the presence of combined stresses requiring the development and use of interaction curves. These complications are further compounded when the skin panels are also required to operate at elevated temperatures which is the case for the specimens which are the subject of this paper.

Time histories of thermal stresses and material yield strength at the middle of the center panel are presented for all three frames in figure 15. A dashed line is faired through the measured axial thermal stresses (the axial direction (x-direction) is parallel to the frames). This data is represented by the circular symbols with the faired dashed line. The axial thermal stresses are computed from the test data using an assumption of uniaxial stress.

The majority of the strain gages were axially oriented single active arm units. No installations were made using a T-gage configuration. There were a nominal number of equiangular rosettes installed so that principal stresses could be calculated. Data from these rosettes is also shown in the form of time histories of principal stresses in figure 15. The angle to the principal stress from the axis of the frame (x-axis) is also presented in time history form in figure 15.

It can be seen by examining figures 15(a) through 15(c) that the principal stresses approach the material yield line in several instances. In the case of Frame C, the principal stress in the 1-direction is only a few percent from the yield line for several minutes. It is also important to note how inappropriate the uniaxial stress assumption is when interpreting this data. The state of stress on the material is considerably more severe than the uniaxially interpreted thermal stresses (circular symbols with the faired dashed line) indicate. The same situation exists to a lesser degree with Frame B (figure 15(b)) where the principal stresses and the material yield are conspicuously close.

The data presented in figure 15 indicates that the center skin panels for two of the three frame sets (Frames B and C) have stress levels very close to the material yield for the heating simulation of the flight. It is important to realize that there are other stresses, such as the stresses due to airloads, that must be superimposed. Hence, after thermal stresses are considered for the skin panels of Frames B and C, there is very little margin left for additional compression stresses from other sources.

The thermal stresses at the middle of an outer skin panel (one of the bays near the edge of the specimen) are presented in figure 16 in a manner similar to the foregoing. Unfortunately, the rosette on the outer skin panel of Frame A failed during the test. Therefore, principal stresses are only available for Frames B and C. It can be seen that the thermal stress situation is not nearly as severe in the outer skin panel as it was in the center skin panel. This probably reflects the relative location of the two panels. The outer skin panel is geometrically located in a position of less restraint (near a boundary of the specimen); hence, the lateral stresses would be expected to be larger.

The angle of principal stress has been shown in both figures 15 and 16. It can be seen that there is a large variation from frame to frame and also a large variation during the time history. This large variation turns out to have little importance if a typical Mohr's Circle of stress is examined. A Mohr's Circle is shown in figure 17 for one of the center skin panels. The circle is quite small indicating that compressive stress changes little regardless of the angle examined. Hence minor errors in the

measurement would be amplified when examining the angle to the principal stress.

Thermal Stress Buckling

A general discussion of the buckling strength of the skin panels for the test specimens (skinned Frames A through C) was presented earlier in the Buckling Analysis Section. An obvious starting point for examining the skin panels is the nature of the edge loading resulting from the thermal stresses. A significant number of axially oriented strain gages was available for viewing the distribution of stress (uniaxial) across the skin of the specimens. The distribution of axial stress across the skins of the specimens at the available strain gages is shown in figure 18. A line is faired through the data to aid the reader in visualizing the general nature of the distribution. The examination of the distribution of stress for the three frames reveals a distinct difference between Frame A and the other two. The axial stress in the skin panels of Frames B and C is completely compressive in nature while the axial stress in Frame A varies between compressive and tension. The introduction of tensile stress in combination with compressive stresses in a plate significantly increases the allowable buckling strength of the skin panel (ref. 26). The thermal stress pattern seen in Frame A (figure 18(a)) is very important in a complex way.

Since a primary element of this paper is to compare the relative merits and performance of the three frame concepts, a simplified approach to evaluating the buckling characteristics is taken. Axial stress measurements are available at the center of all three panels across the section of the specimens. This is the most complete and consistent measurement available for general evaluation. Time histories of the axial thermal stress (uniaxially assumed) at the center of the three skin panels for the three frame concepts is presented in figure 19. The thermal stress is represented by the circular symbols with the faired dashed line. Time histories of the estimated buckling strength of the skin panels are also presented. A band of buckling strength is shown in figure 19 ranging from simply supported frame edges ($K = 2.52$, equation (8)) to clamped frame edges ($K = 4.24$, equation (9)). Figure 19 depicts if and when the buckling of the individual skin panels occurs. The reader must remember that the panel edge loading (the thermal stresses) tends to relieve itself if an instability occurs. Hence, the progression of buckling in the classic sense does not occur for panels loaded by only thermal stresses.

Consistent with previous observations, the thermal stresses in Frame A are not excessively large as presented in figure 19(a). One outer skin panel indicates sufficient thermal stress to cause an instability. It must be borne in mind, however, that the

presence of tensile thermal stresses in the skin of Frame A might significantly increase the predicted buckling strength of this skin panel. The axial thermal stresses in the skin panels of Frame B clearly exceed the predicted buckling strength for a major portion of the heating time. The measured axial thermal stresses of Frame C also penetrated the buckling region, although not to the degree that was observed for Frame B. Information to verify or substantiate the instability of the skin panels is marginal since conventional approaches such as examining load versus deformation (or strain) are inappropriate.

The most substantive verification of instability can be seen by examining figure 20 with respect to figure 19(c). In figure 19(c), it can be seen that the earliest implied instability occurs in the center panel. A major instability in the center panel appears to have occurred in figure 20(c) at the three minute time. What is observed in the progression from figure 20(b) to 20(c) is a huge bulge in the stress distribution of the center panel near the frame. The bulge is still present in figure 20(d) although the stress has obviously been redistributed.

It is curious to note how the buckling strength changes when the stress pattern is biaxial rather than uniaxial. The test data presented for the middle panel in figure 19(b) is shown in figure 21. The two bands represent one for buckling due to a uniaxial stress state and the other for a biaxial stress state. Obviously it would involve a significant error to assume a state of uniaxial (extensional) stress in the circumferential direction (hoop stress) of a fuselage frame.

Predicted Skin Thermal Stress

The previously discussed NASTRAN models were utilized in preparing a comparison between the experimentally measured thermal stresses and the predictions for the three frames. A time history of thermal stress is presented in figure 22 for the sum of the thermal stress at the center of the three panels divided by the number of panels (three) at that cross section. This type of presentation would normally not be of much importance since data is preferably presented for discrete points on the structure. However, the implied instability of the skin panels detracts from the significance of that type of comparison and a more general examination is more enlightening. It can be seen in figure 22 that the comparison of the measured and predicted values is not particularly good for the three frame configurations. It is especially bad for Frame B. This tends to correlate with previous observations about the severity of the thermal stresses in Frame B.

The correlation between measured thermal stresses and calculated thermal stresses can be seen in more specific terms in figure 23 for a single time segment. Previous observations are generally substantiated in the three comparisons of figure 23. Six out of the nine (67 percent) data points for Frame A (figure 23(a)) correlate well with the predicted curve. Only four out of ten (40 percent) of the data points for Frame B correlate well with the predicted curve. The data points for Frame C correlate even worse with the predicted curve because only three out of twelve (25 percent) correlate well. The correlation between measured thermal stresses and calculated thermal stresses is not good. It is particularly bad for Frames B and C. Part of this lack of correlation can be attributed to the assumption of uniaxial stress in the NASTRAN modeling. The majority of the lack of correlation should be attributed to the state of impending elastic instability, particularly in Frames B and C, resulting from excessive thermal stresses and thermally degraded cross-sectional rigidity. This observation is fairly straightforward when figures 18 through 23 are considered in aggregate.

CONCLUDING REMARKS

Laboratory heating tests simulating Mach 6 flight were conducted on three frame/skin specimens: (1) a titanium truss frame with a Lockalloy skin, (2) a stainless steel Z-frame with a Lockalloy skin, and (3) a titanium Z-frame with a Lockalloy skin. The most severe thermal stresses occurred on the specimen with the stainless steel frame. The integrity of this specimen was threatened from thermal stresses approaching the yield strength of the material and thermal stresses exceeding the buckling strength of the skin panels. The same situation existed, but to a lesser degree, for the specimen with the titanium Z-frame. The large magnitude of thermal stresses observed for these two specimens allowed little margin for the structure to carry other types of loads.

The specimen configured with a titanium truss frame consistently had lower levels of thermal stresses than the other two specimens. The overall integrity of this specimen was considerably less threatened by the thermal heating test. The structural weight of this specimen was eight to ten percent heavier than the other two specimens. The thermal stresses for all the specimens were of dominating proportions with respect to structural design. The state of thermal stress in the skins was clearly biaxial in nature.

The correlation of measured thermal stresses with calculated thermal stresses using a NASTRAN model was generally poor for the

skin areas and good for the frames. The poor correlation in the skin areas was attributed to: (1) an inappropriate assumption of uniaxial stress for the NASTRAN models, and (2) a state of elastic instability (thermal buckling) occurring during a major portion of the heating of the specimens. The correlation in the skin areas for the specimen with the titanium truss frame was better than for the other two specimens because the skin thermal stresses were probably below the unstable level of the skin panels.

Dryden Flight Research Center
National Aeronautics and Space Administration
Edwards, Calif., October 20, 1980

REFERENCES

1. Stone, J. E.; and Koch, L. C.: Hypersonic Airframe Structures Technology Needs and Flight Test Requirements. NASA CR-3130, 1979.

2. Plank, P. P.; Sakata, I. F.; Davis, G. W.; and Richie, C. C.: Hypersonic Cruise Vehicle Wing Structure Evaluation. NASA CR-1568, 1970.

3. Plank, P. P.; and Penning, F. A.: Hypersonic Wing Test Structure Design, Analysis, and Fabrication. NASA CR-127490, 1973.

4. Kelly, H. Neale; Rummler, Donald R.; and Jackson, L. Robert: Research in Structures and Materials for Future Space Transportation Systems - An Overview. AIAA Paper No. 79-0859, May 1979.

5. Plank, P. Paul; and Phillips, Lawrence P.: Materials Applications and Structural Concepts for Hypersonic Air-Induction Systems. SAE Paper No. 690664, Oct. 1969.

6. Kelly, H. Neale; Wieting, Allan R.; Shore, Charles P.; and Nowak, Robert J.: Recent Advances in Convectively Cooled Engine and Airframe Structures for Hypersonic Flight. NASA CP-2065, Part I, 1978, pp. 47-61.

7. Watts, J. D.; Jackson, L. R.; and Hunt, J. L.: Hypersonic Structures: An Aerodynamicist's Perspective. NASA CP-2065, Part I, 1978, pp. 5-38.

8. Quinn, Robert D.; and Olinger, Frank V. (appendix by James C. Dunavant and Robert L. Stallings, Jr.): Heat-Transfer Measurements Obtained on the X-15 Airplane Including Correlations With Wind-Tunnel Results. NASA TM X-1705, 1969.

9. Andrews, William H.: Summary of Preliminary Data Derived From the XB-70 Airplanes. NASA TM X-1240, 1966.

10. Quinn, Robert D.; and Olinger, Frank V.: Flight Temperatures and Thermal Simulation Requirements. NASA YF-12 Flight Loads Program, NASA TM X-3061, 1974, pp. 145-183.

11. Jenkins, J. M.; Field, R. A.; and Sefic, W. J.: Elevated-temperature Effects on Strain Gages on the YF-12A Wing. Experimental Mech., vol. 19, no. 3, March 1979, pp. 81-86.

12. Thornton, Earl A.; and Wieting, Allan R.: Recent Advances in Thermostructural Finite Element Analysis. NASA CP-2065, Part II, 1978, pp. 851-896.

13. Adelman, Howard M.; and Robinson, James C.: Recent Advances in Thermal-Structural Analysis and Design. NASA CP-2065, Part II, 1978, pp. 897-941.

14. Combs, H. G., et al.: Configuration Development Study of the X-24C Hypersonic Research Airplane - Executive Summary. NASA CR 145274, 1977.

15. Jenkins, Jerald M.; Schuster, Lawrence S.; and Carter, Alan L.: Correlation of Predicted and Measured Thermal Stresses on a Truss-Type Aircraft Structure. NASA TM-72857, 1978.

16. Jenkins, Jerald M.: Correlation of Predicted and Measured Thermal Stresses on an Advanced Aircraft Structure With Similar Materials. NASA TM-72862, 1979.

17. Jenkins, Jerald M.: Correlation of Predicted and Measured Thermal Stresses on an Advanced Aircraft Structure With Dissimilar Materials. NASA TM-72865, 1979.

18. McCormick, Caleb W., ed.: The NASTRAN User's Manual (Level 15). NASA SP-222(01), 1972.

19. Stillwell, Wendell L.: X-15 Research Results With a Selected Bibliography. NASA SP-60, 1965.

20. Jenkins, Jerald M.; Tang, Ming H.; and Pearson, George P. E.: Vertical-Tail Loads and Control-Surface Hinge-Moment Measurements on the M2-F2 Lifting Body During Initial Subsonic Flight Tests. NASA TM X-1712, 1968.

21. Tang, Ming H.; and Pearson, George P. E.: Flight-Measured HL-10 Lifting Body Center Fin Loads and Control Surface Hinge Moments and Correlation With Wind-Tunnel Predictions. NASA TM X-2419, 1971.

22. Tang, Ming H.; and DeAngelis, V. Michael: Fin Loads and Control-Surface Hinge Moments Measured in Full-Scale Wind-Tunnel Tests on the X-24A Flight Vehicle. NASA TM X-1922, 1969.

23. Sefic, Walter J.; and Anderson, Karl F.: NASA High Temperature Loads Calibration Laboratory. NASA TM X-1868, 1969.

24. Marin, Joseph; and Sauer, John A.: Strength of Materials. The Macmillan Co., New York, 1960.

25. Gerard, George; and Becker, Herbert: Handbook of Structural Stability. Part I - Buckling of Flat Plates. NACA TN-3781, 1957.

26. Timoshenko, Stephen P.; and Gere, James M.: Theory of Elastic Stability. McGraw-Hill Book Co., Inc., 1961.

27. Wang, Chi-Teh: Applied Elasticity. McGraw-Hill Book Co., Inc., 1953.

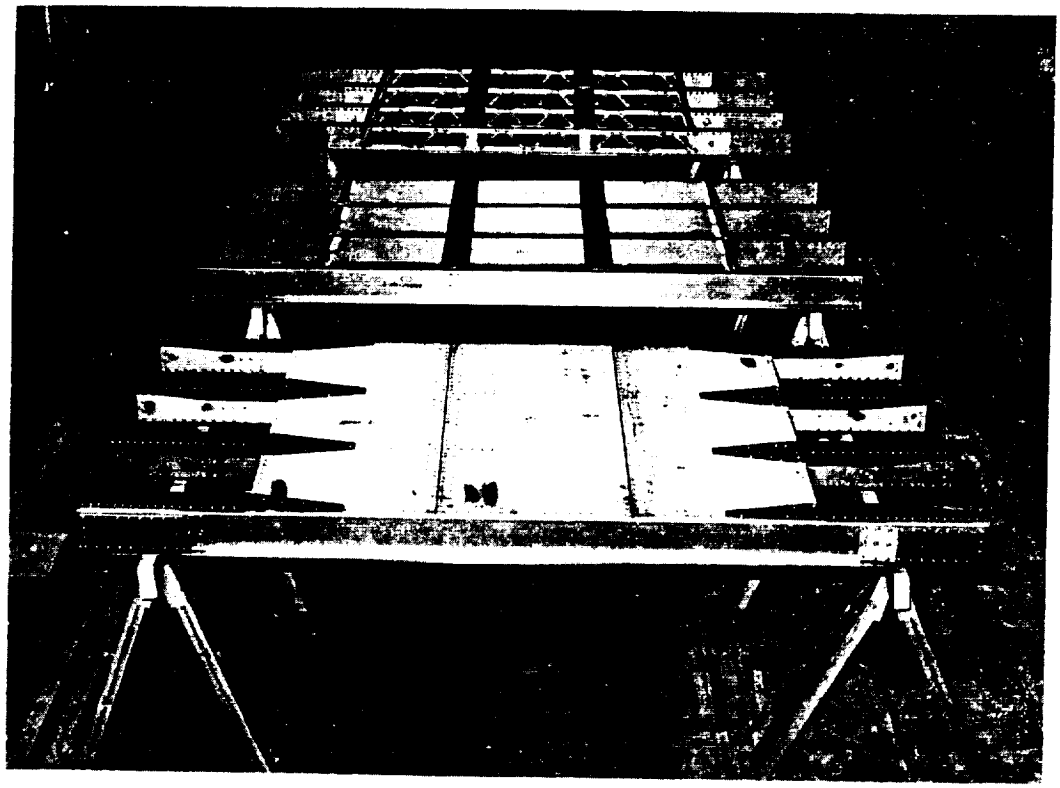

ES 31362

Figure 1. Test specimens.

ES 31365

Figure 2. Titanium truss frame structure identified as Frame A.

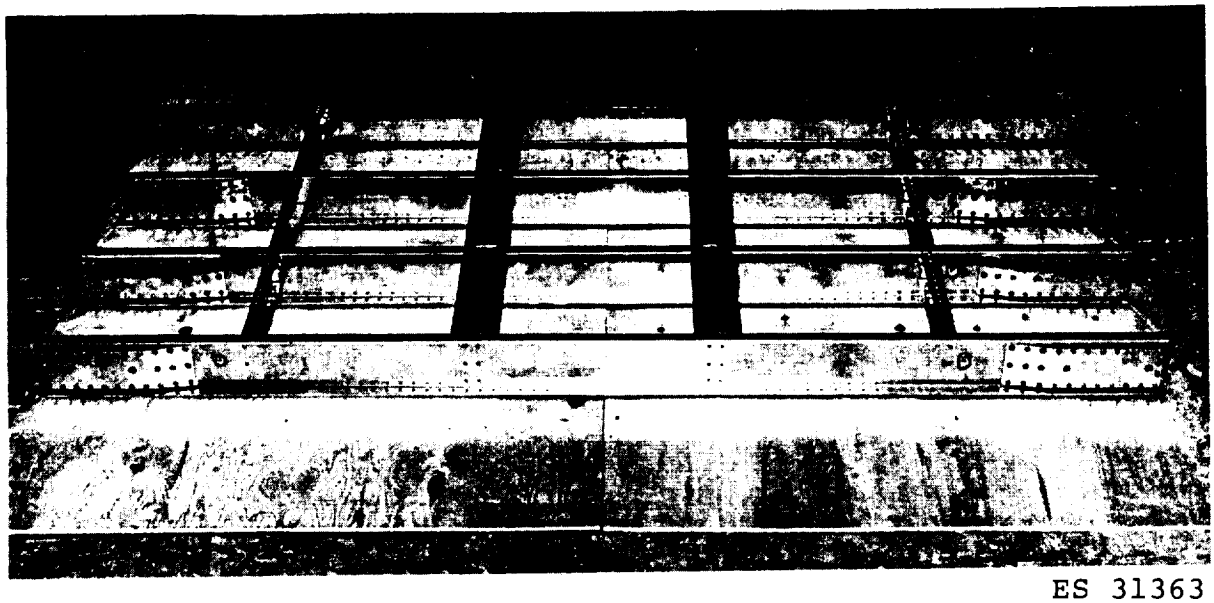

ES 31363

Figure 3. Stainless steel Z-frame structure identified as Frame B.

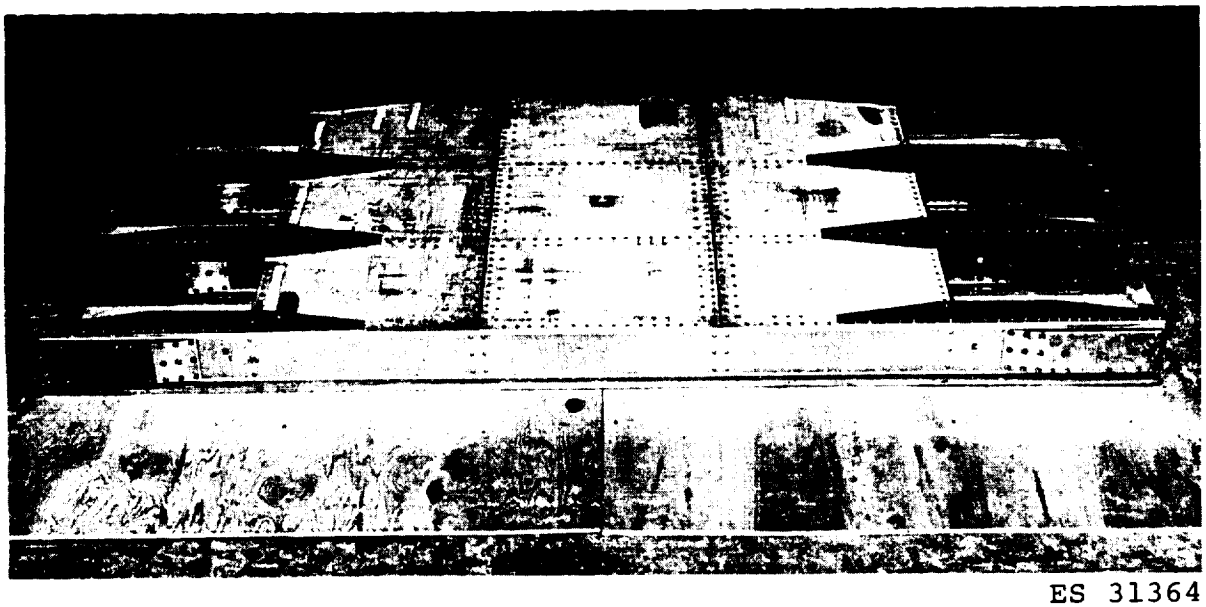

ES 31364

Figure 4. Titanium Z-frame structure with skins attached identified as Frame C.

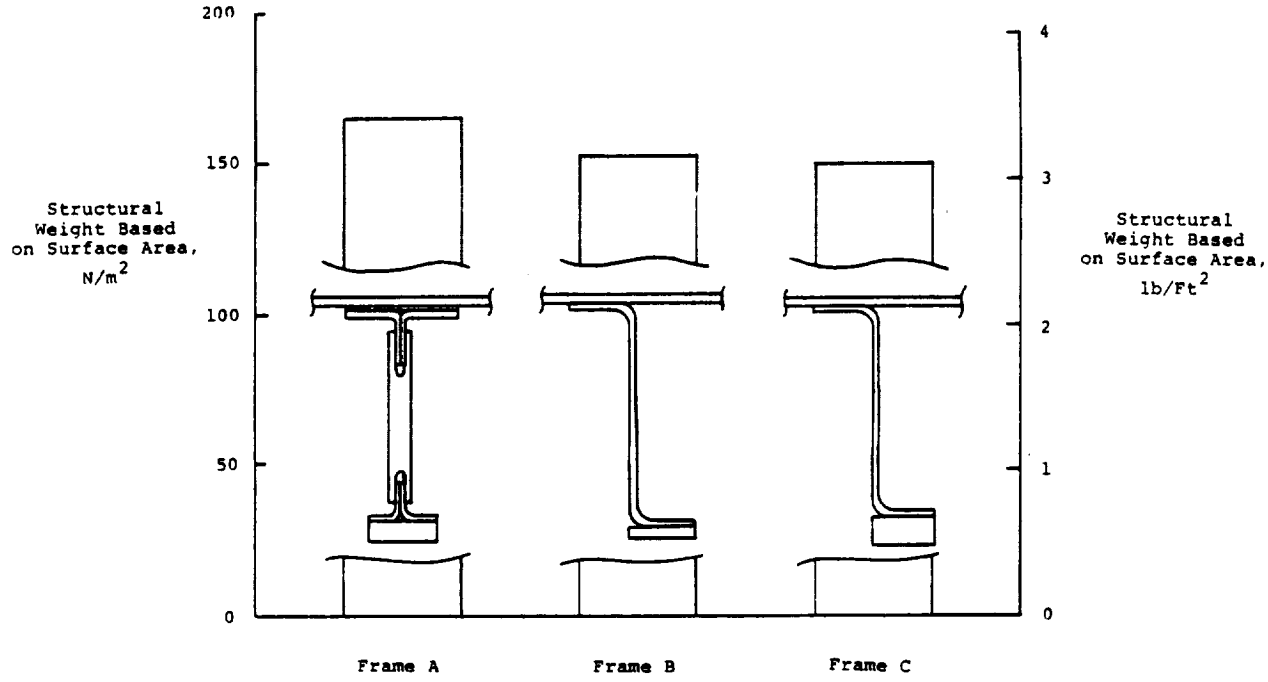

Figure 5. A comparison of the relative weights of the three frame structures.

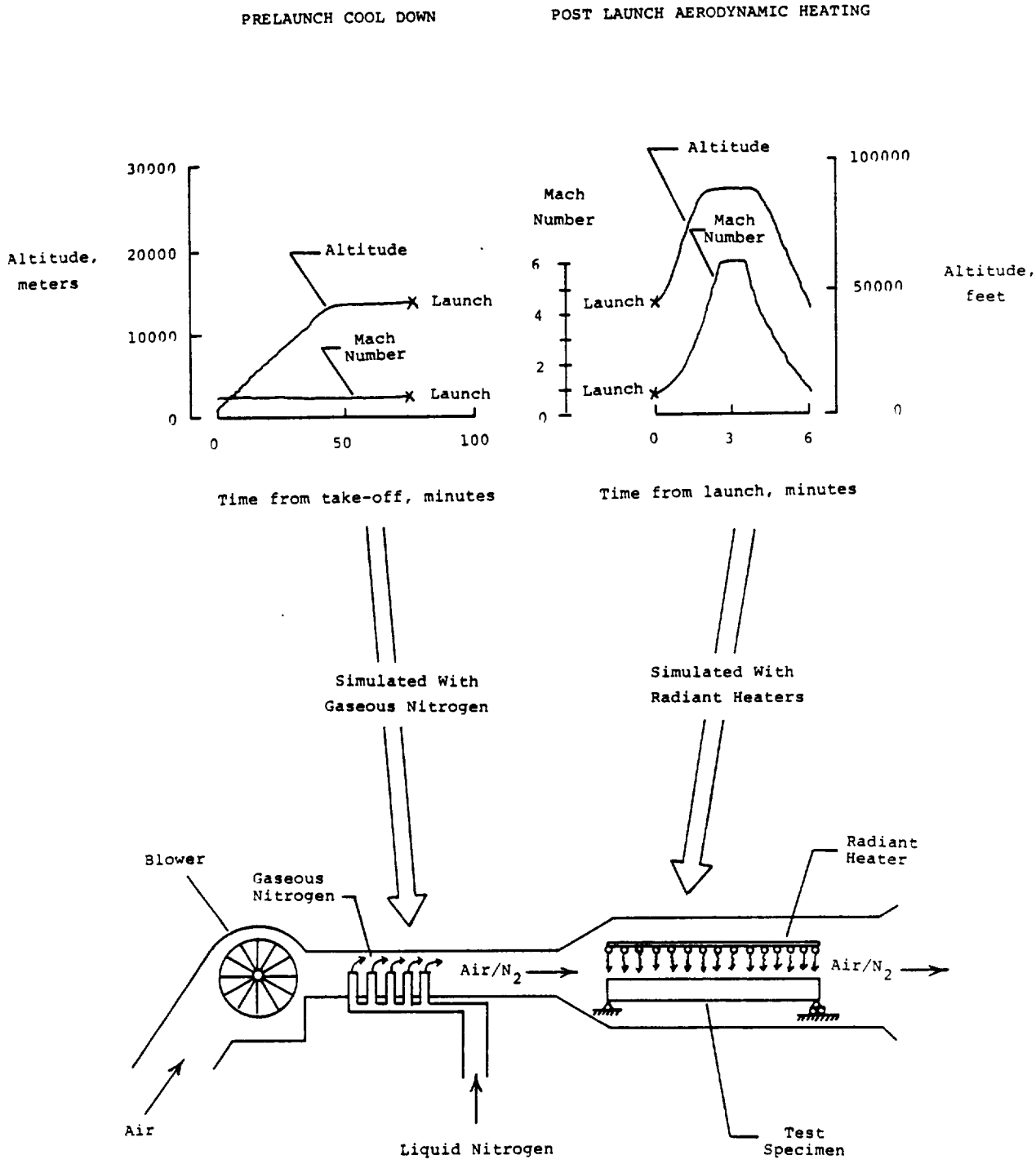

Figure 6. A depicted illustration of the heating simulation of a high speed flight.

ES 32743

Figure 7. Radiant heater showing the quartz lamps and reflectors.

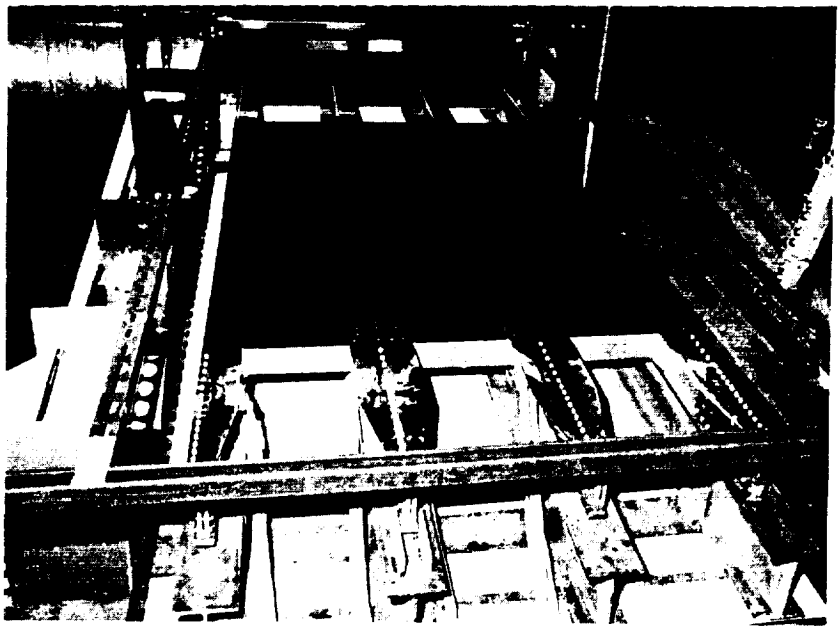

ES 32742

Figure 8. Test specimen with the nitrogen ducting in the background.

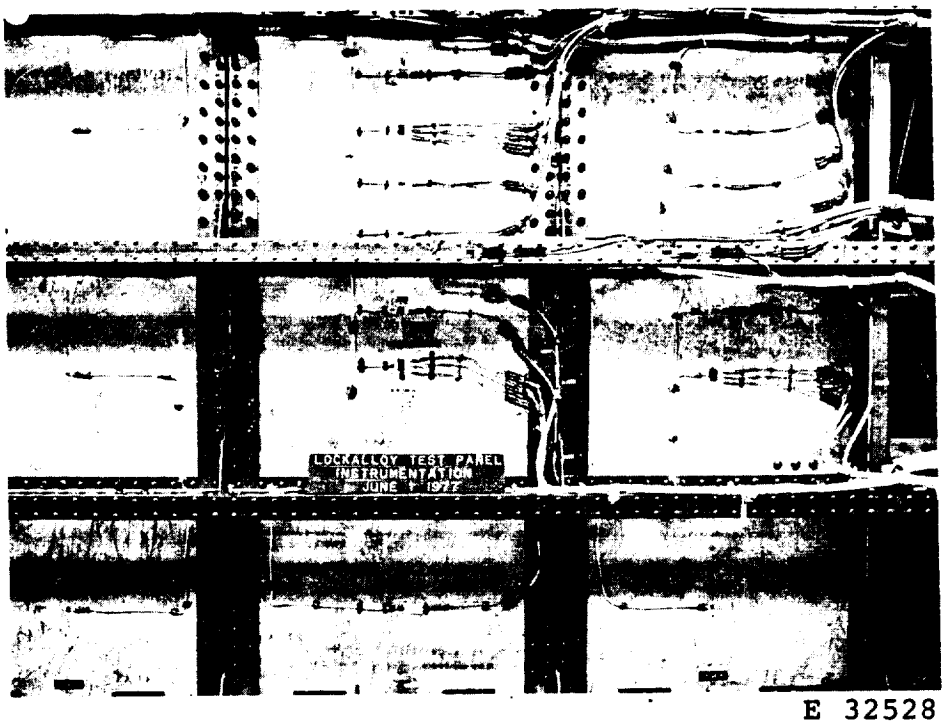

E 32528

Figure 9. Overall view of the strain gages and thermocouples.

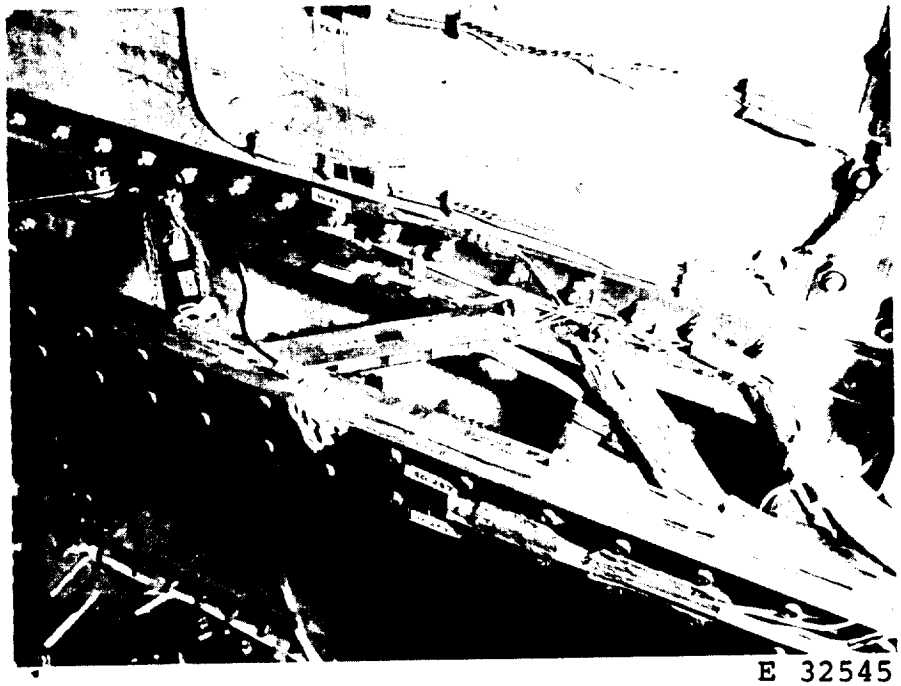

E 32545

Figure 10. Detailed view of the strain gages and thermocouples.

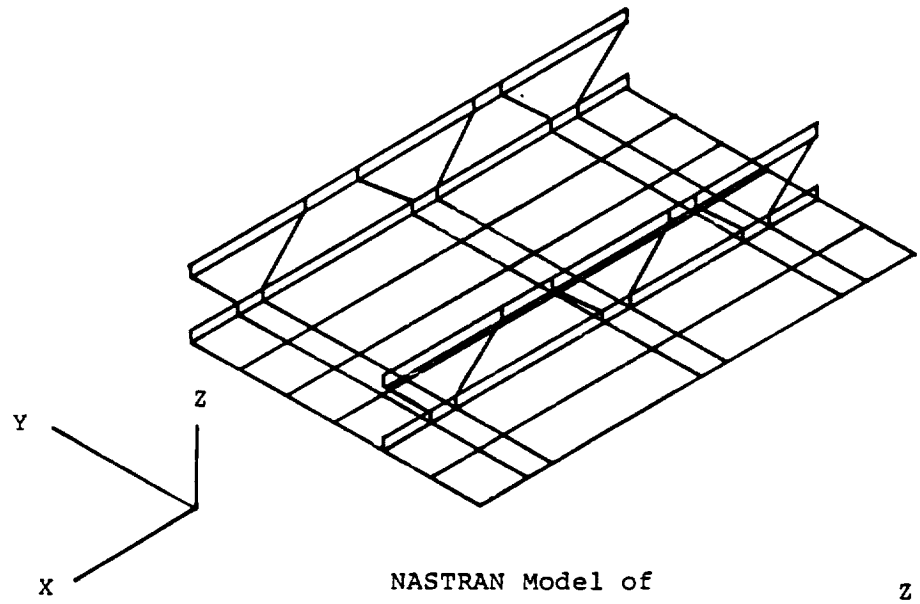

NASTRAN Model of
Frame A

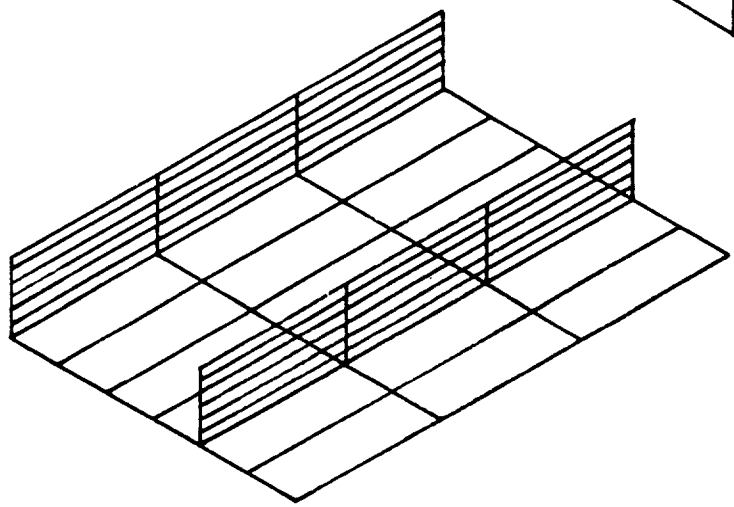

NASTRAN Model of
Frames B and C

Figure 11. Sketch of NASTRAN models used for analysis.

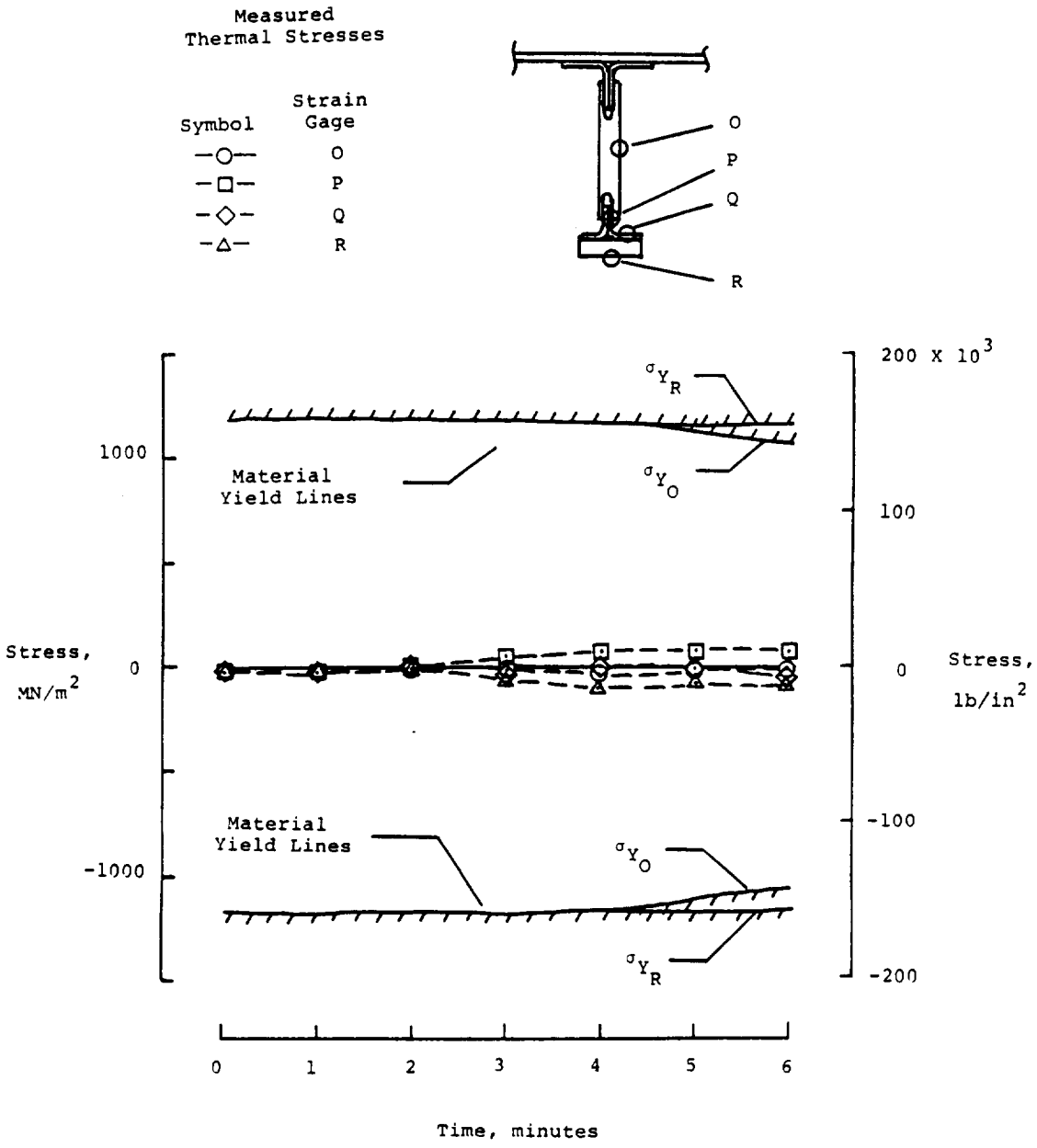

(a) Frame A.

Figure 12. Time histories of frame axial thermal stresses compared to material yield strengths.

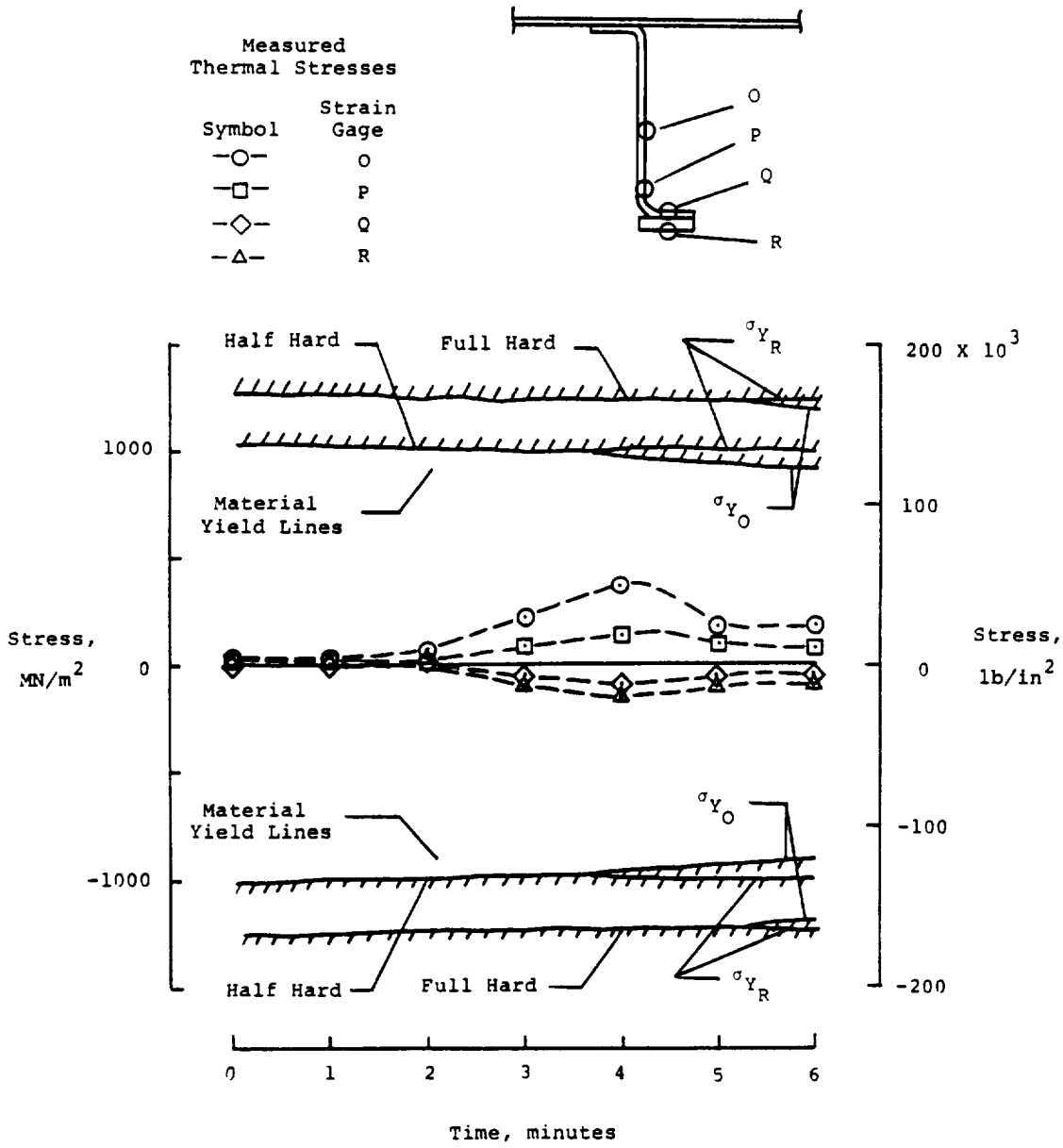

(b) Frame B.

Figure 12. Continued.

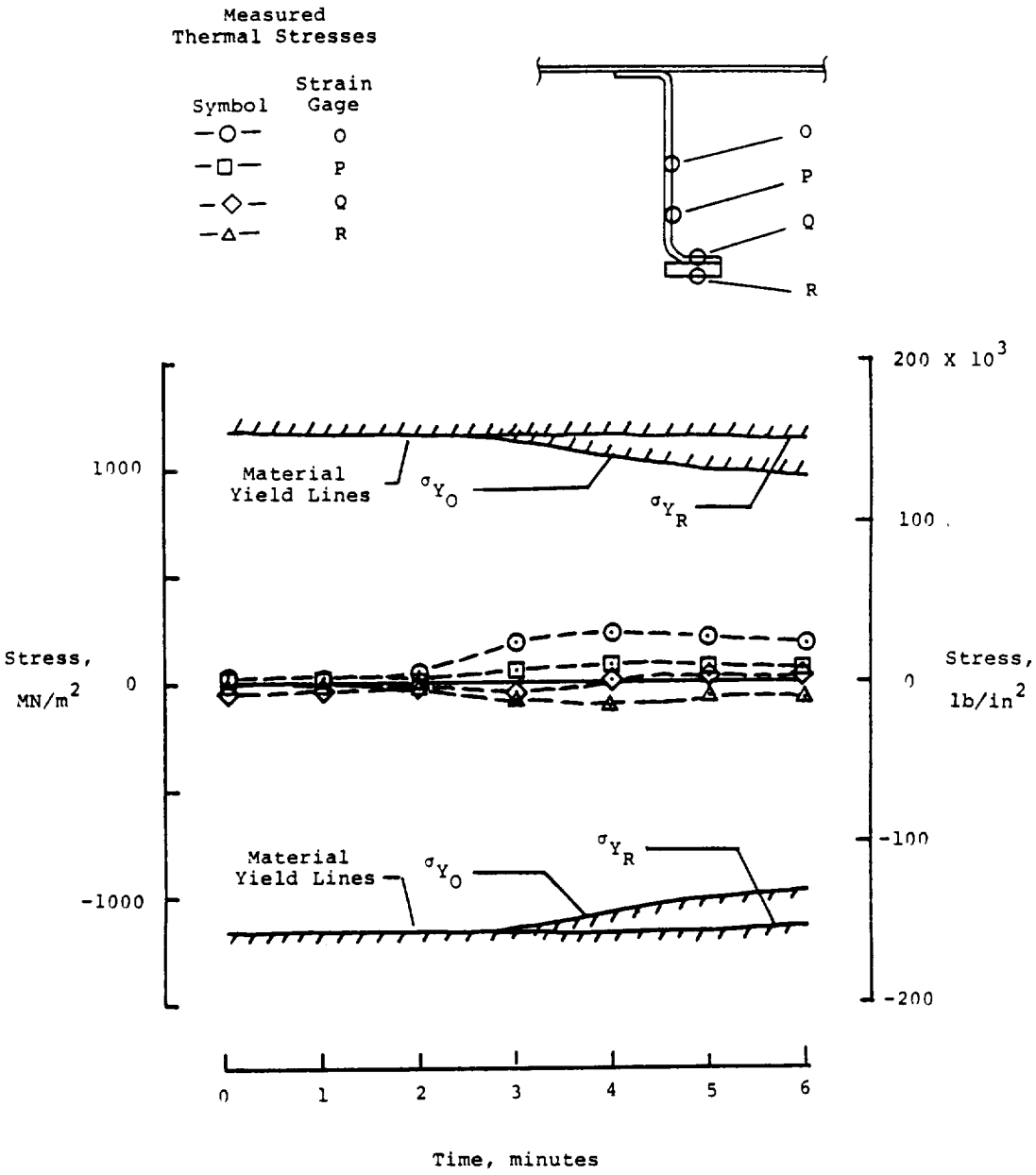

(c) Frame C.

Figure 12. Concluded.

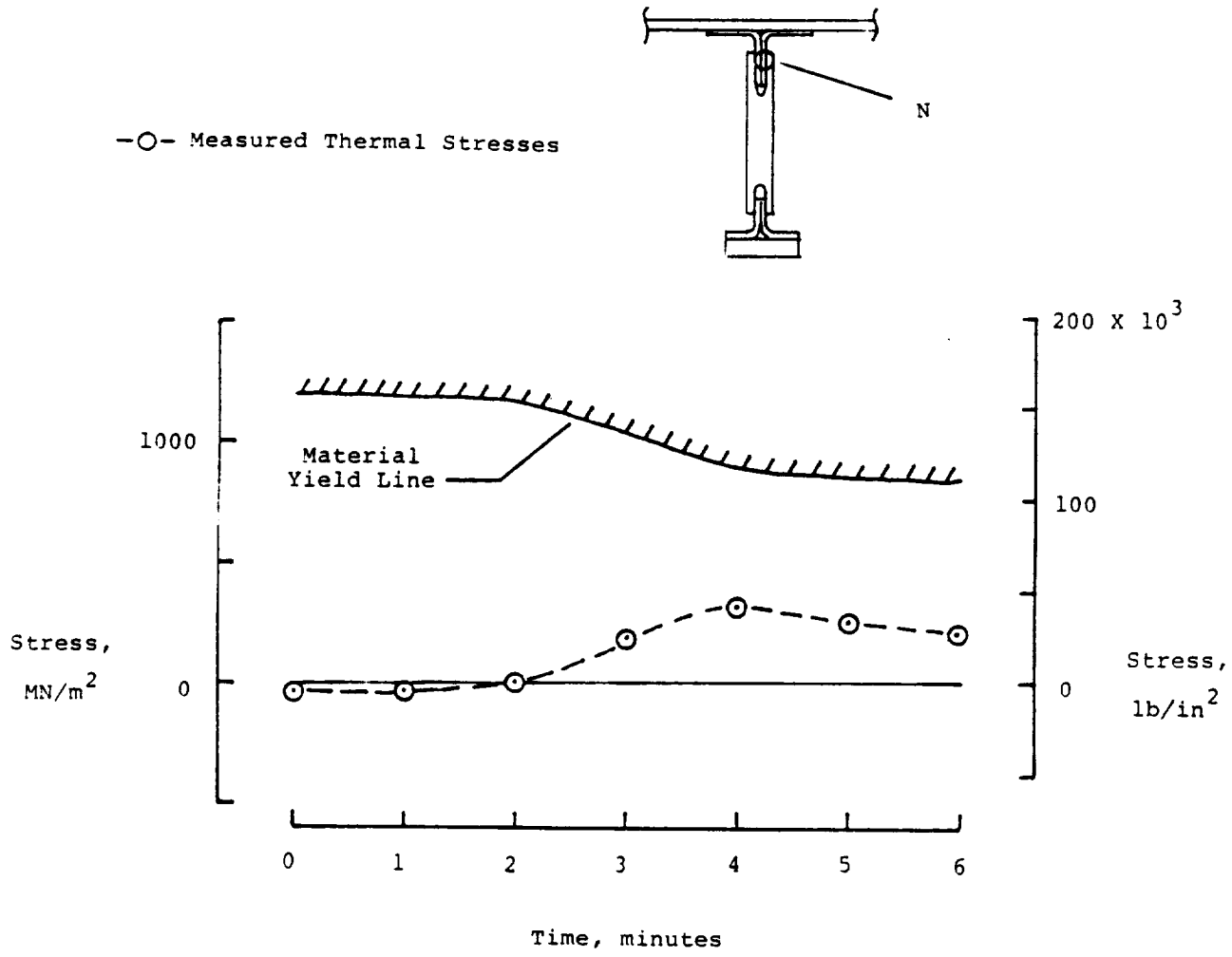

(a) Frame A.

Figure 13. Time histories of frame axial thermal stresses compared to material yield strengths.

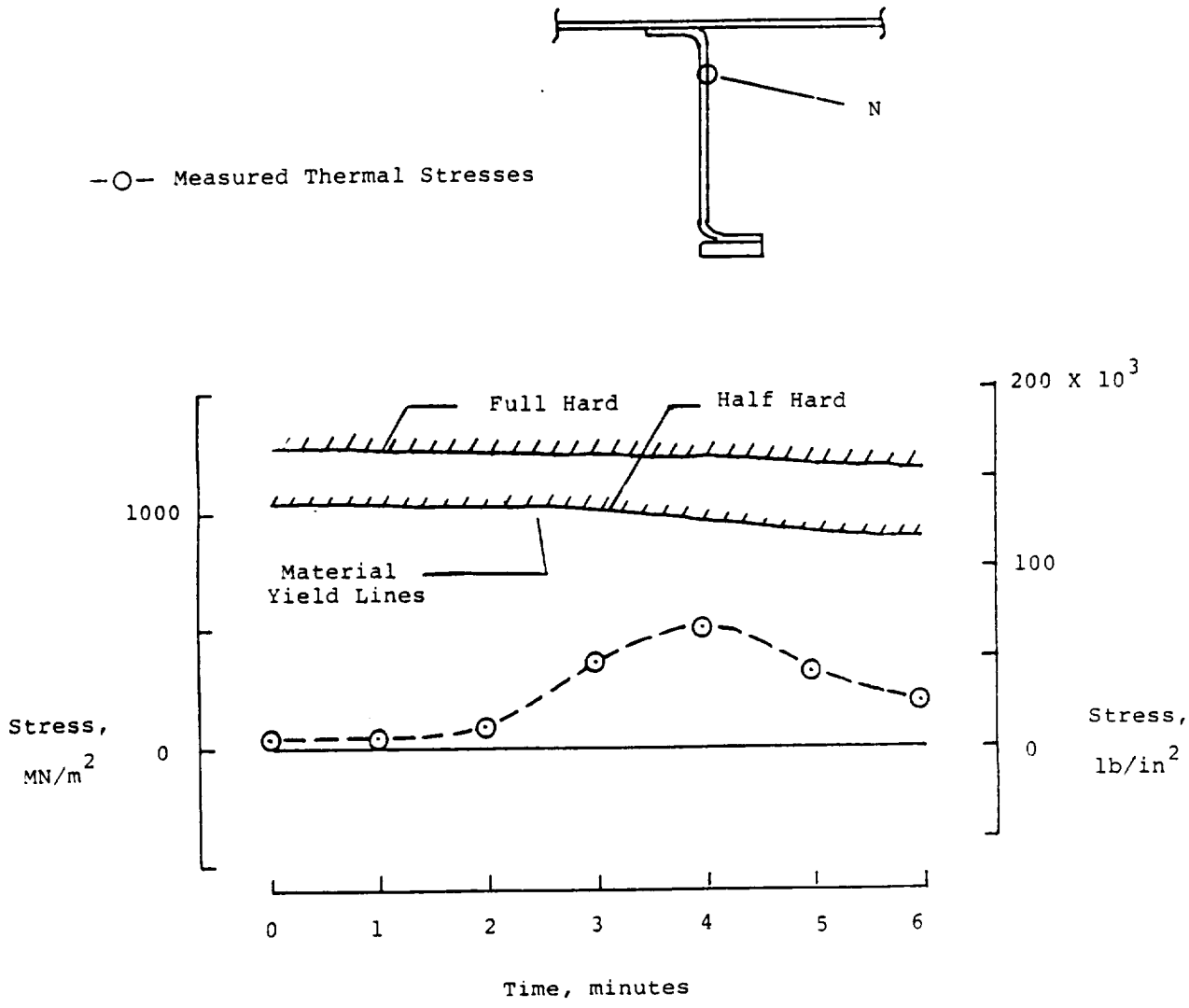

(b) Frame B.

Figure 13. Continued.

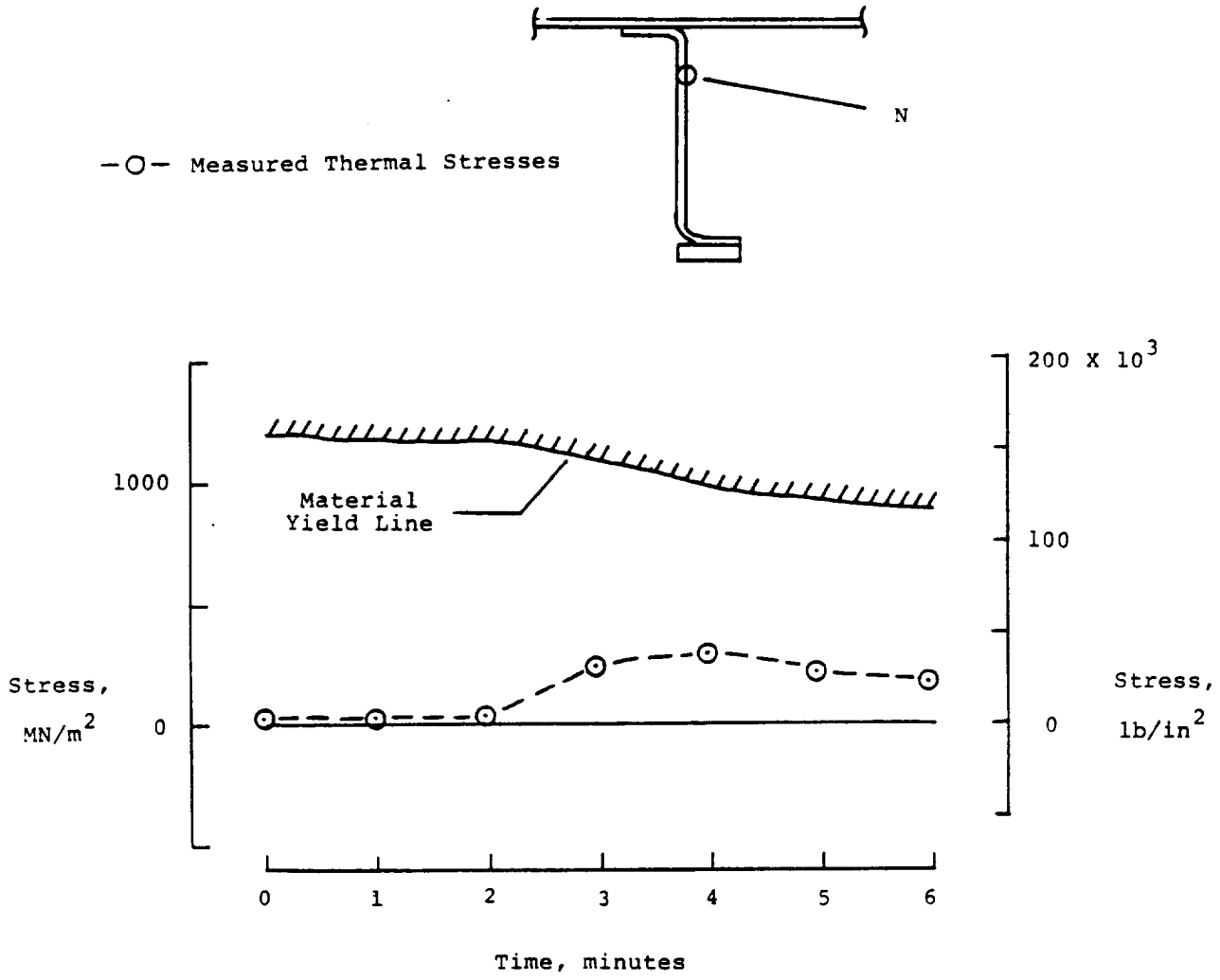

(c) Frame C.

Figure 13. Concluded.

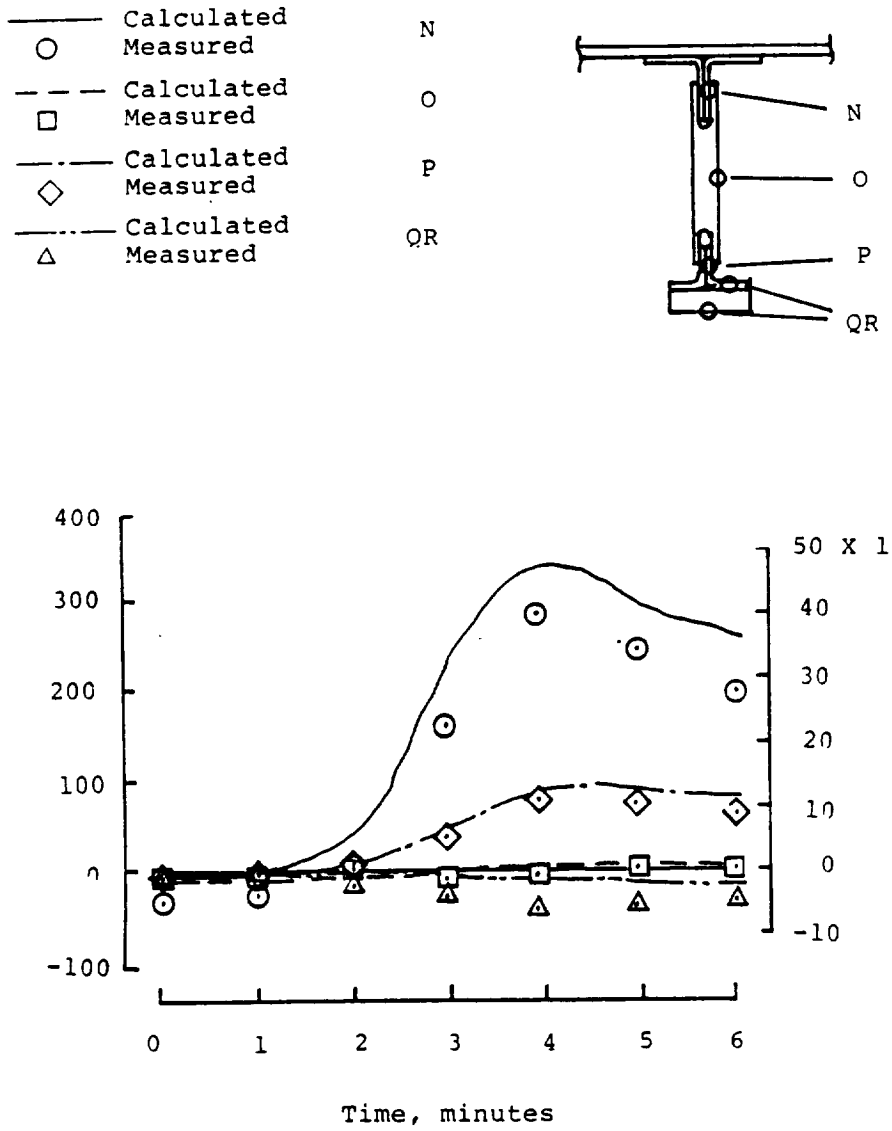

(a) Frame A.

Figure 14. Comparison of time histories of calculated and measured frame axial thermal stresses.

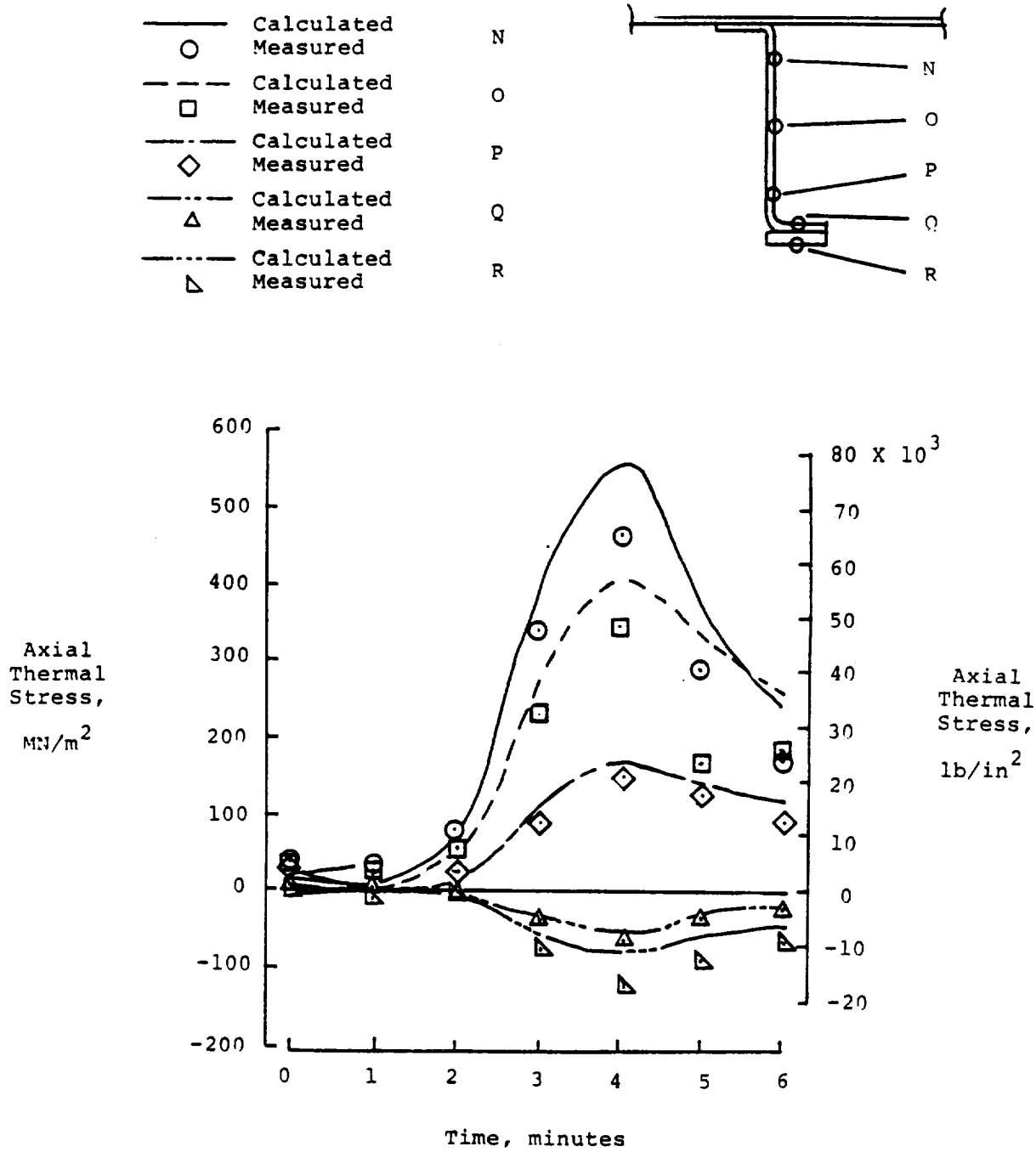

(b) Frame B.

Figure 14. Continued.

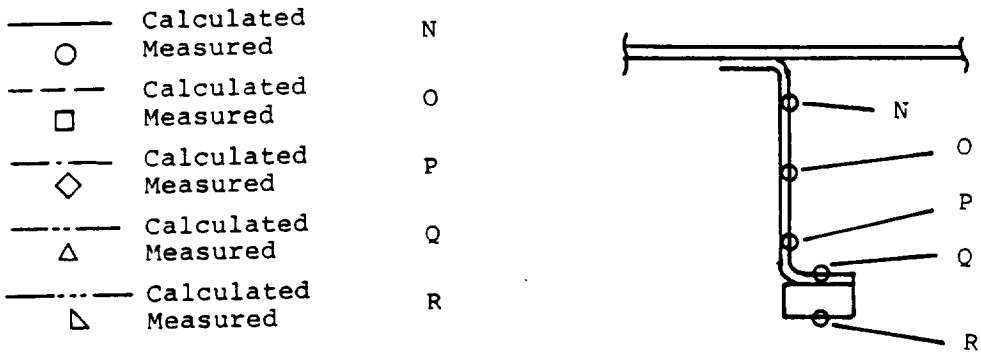

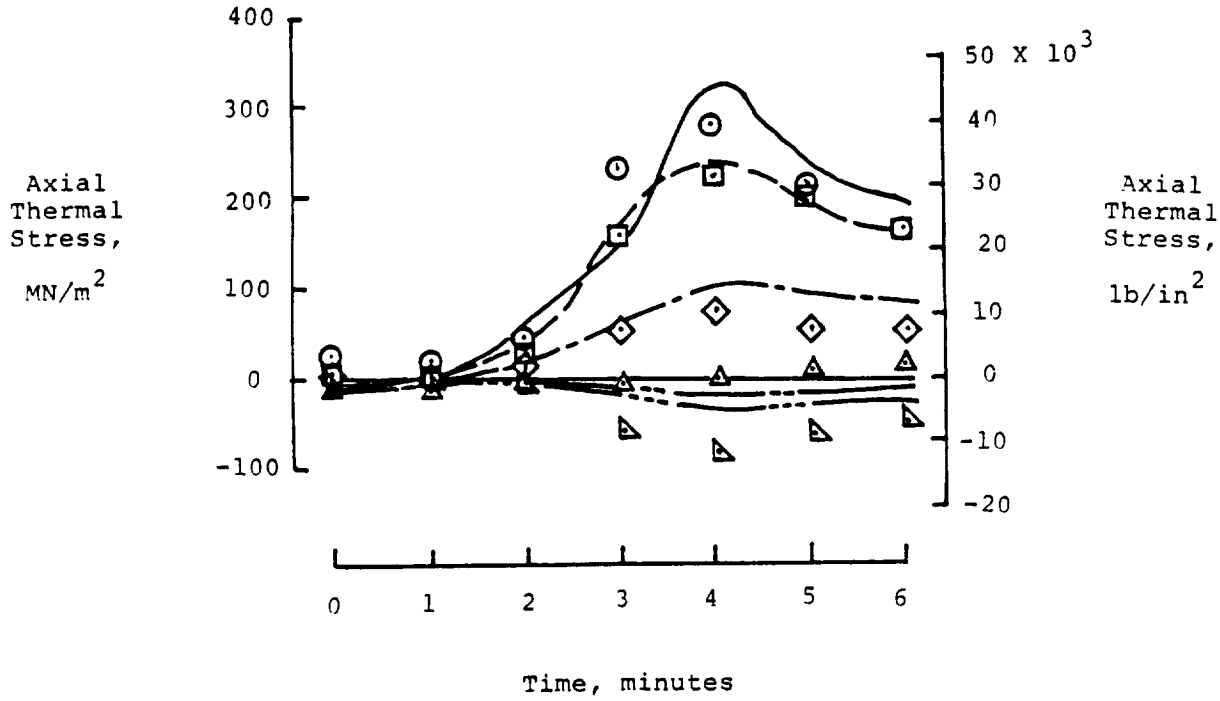

(c) Frame C.

Figure 14. Concluded.

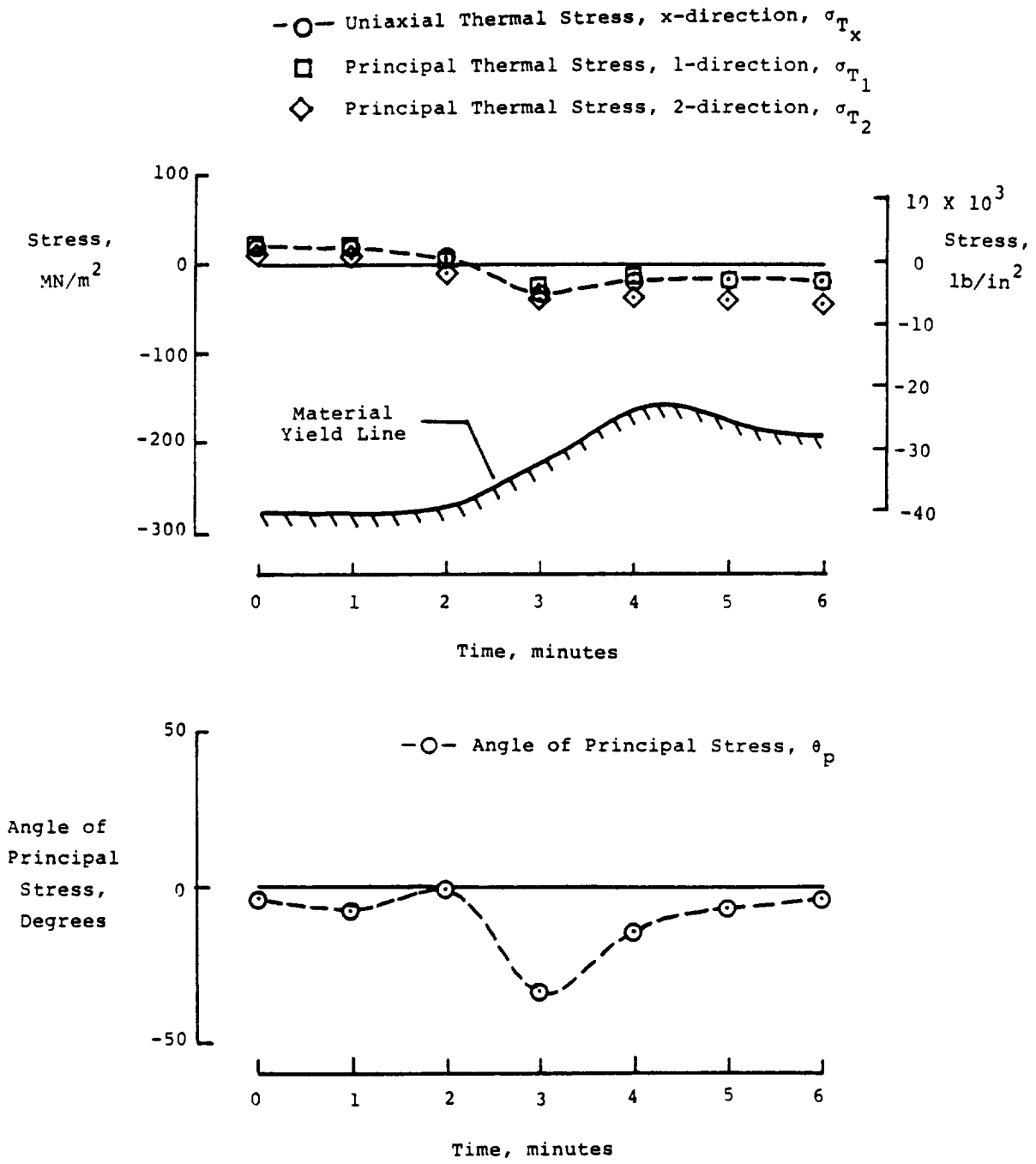

(a) Frame A.

Figure 15. Time histories of skin thermal stresses compared to material yield strengths for a middle panel.

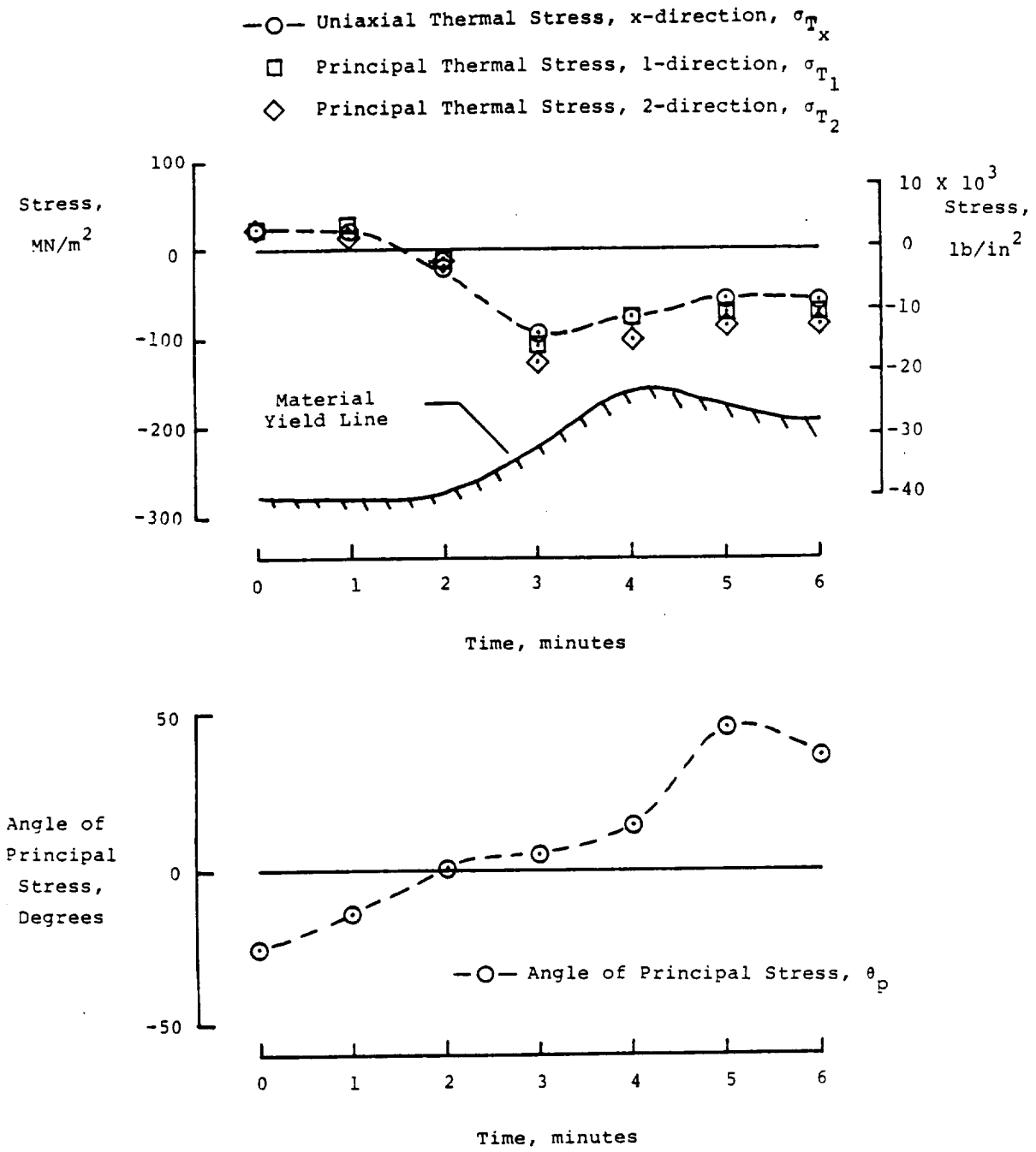

(b) Frame B.

Figure 15. Continued.

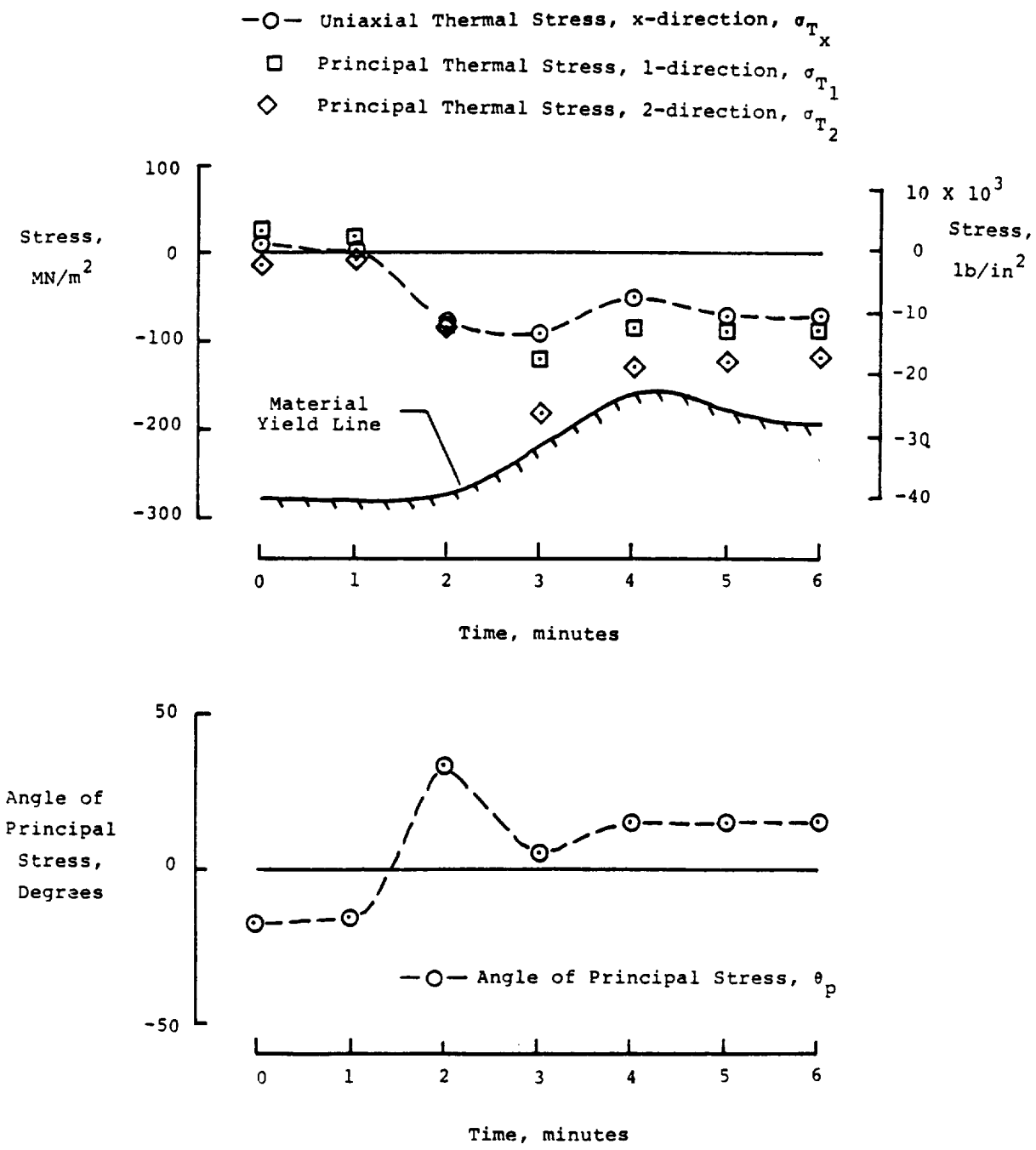

(c) Frame C.

Figure 15. Concluded.

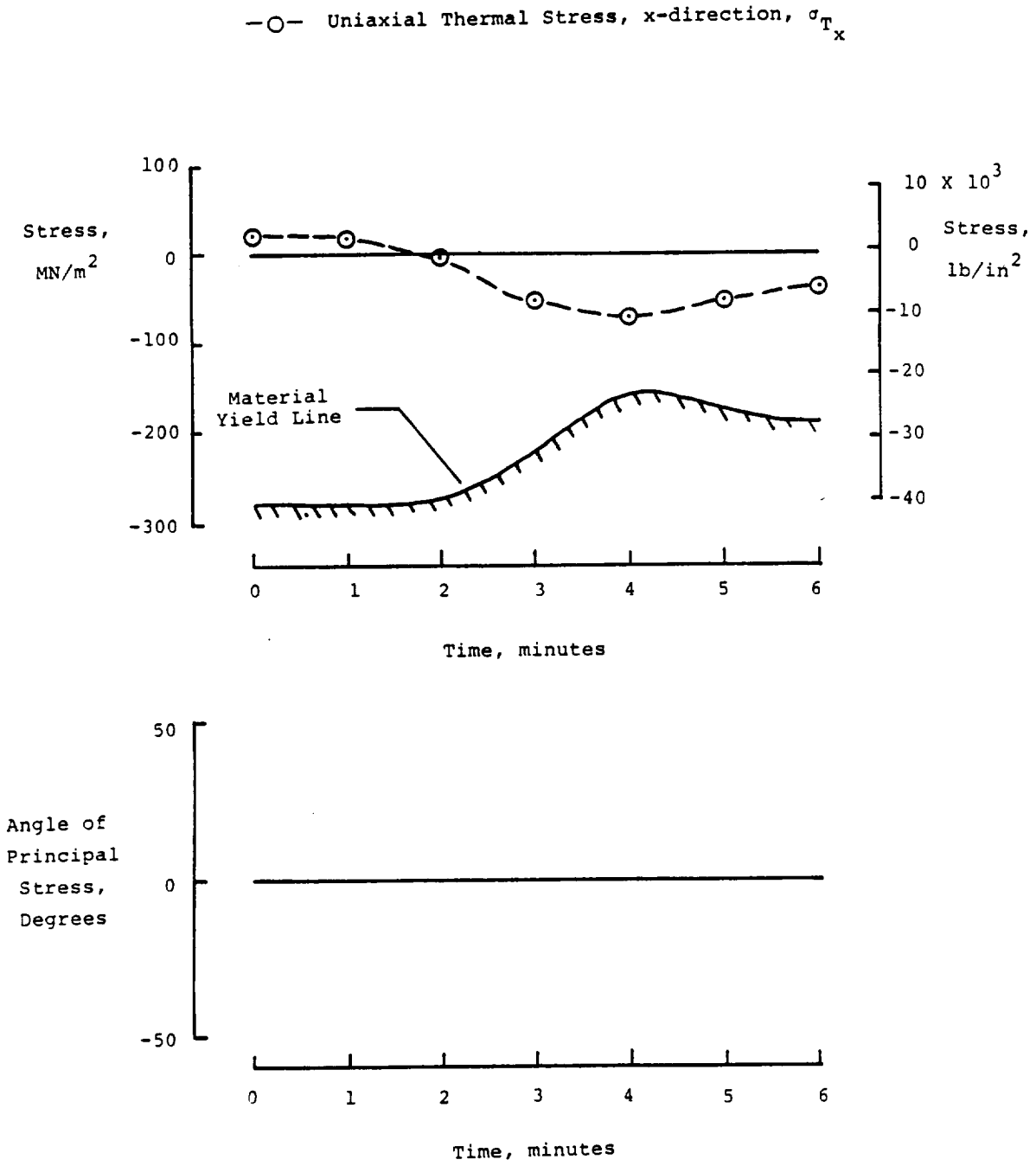

(a) Frame A.

Figure 16. Time histories of skin thermal stresses compared to material yield strengths for an outer panel.

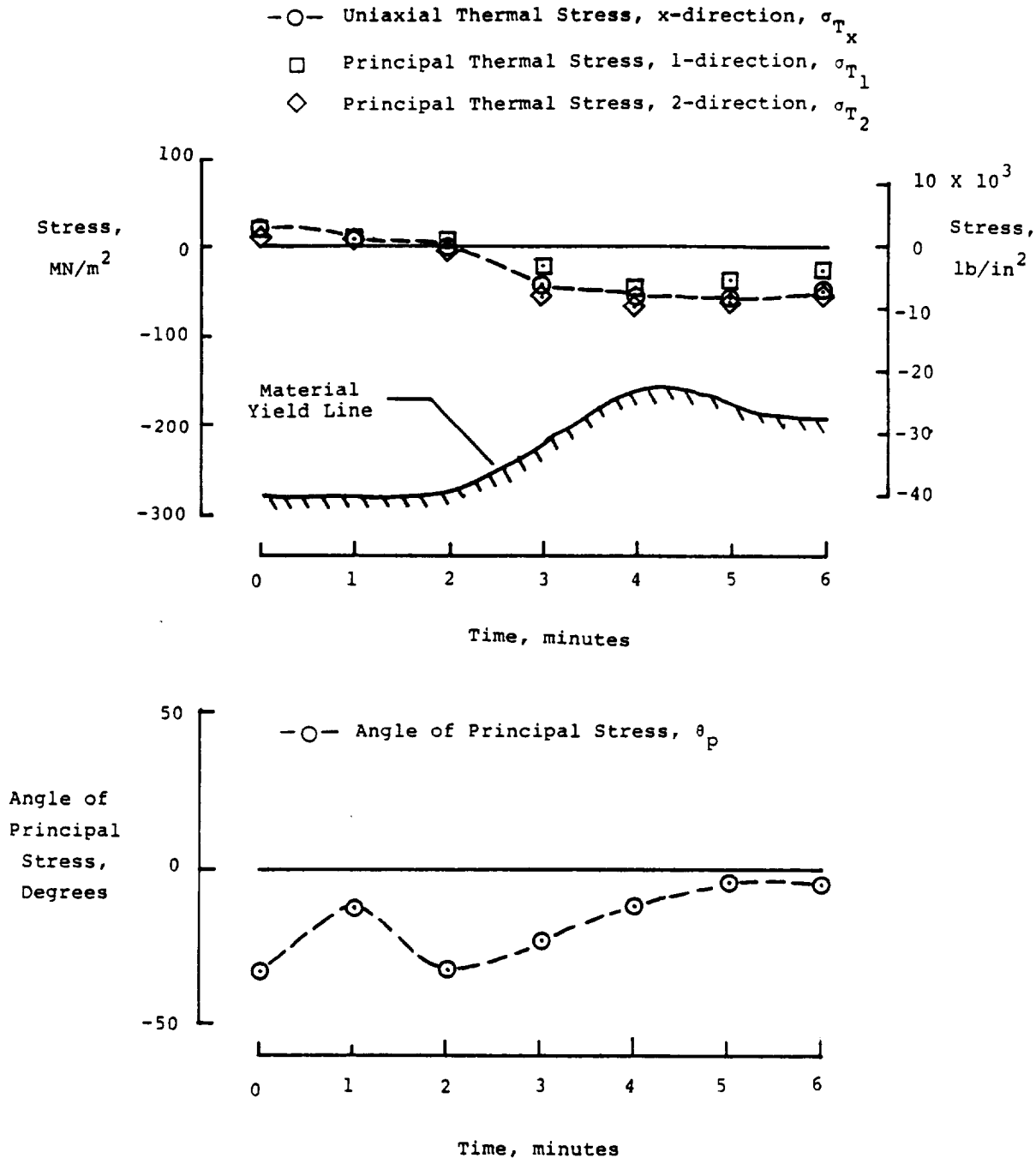

(b) Frame B.

Figure 16. Continued.

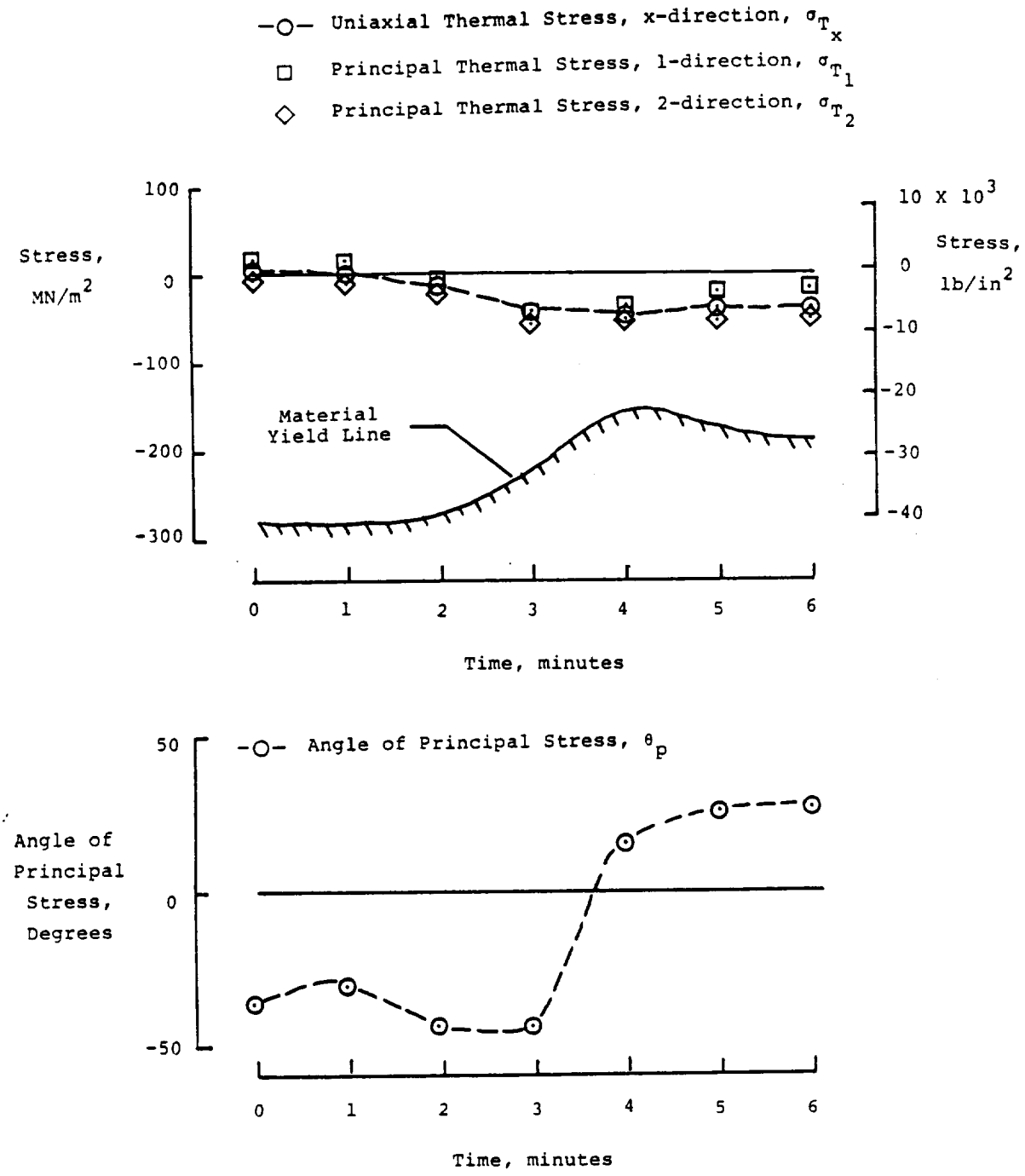

(c) Frame C.

Figure 16. Concluded.

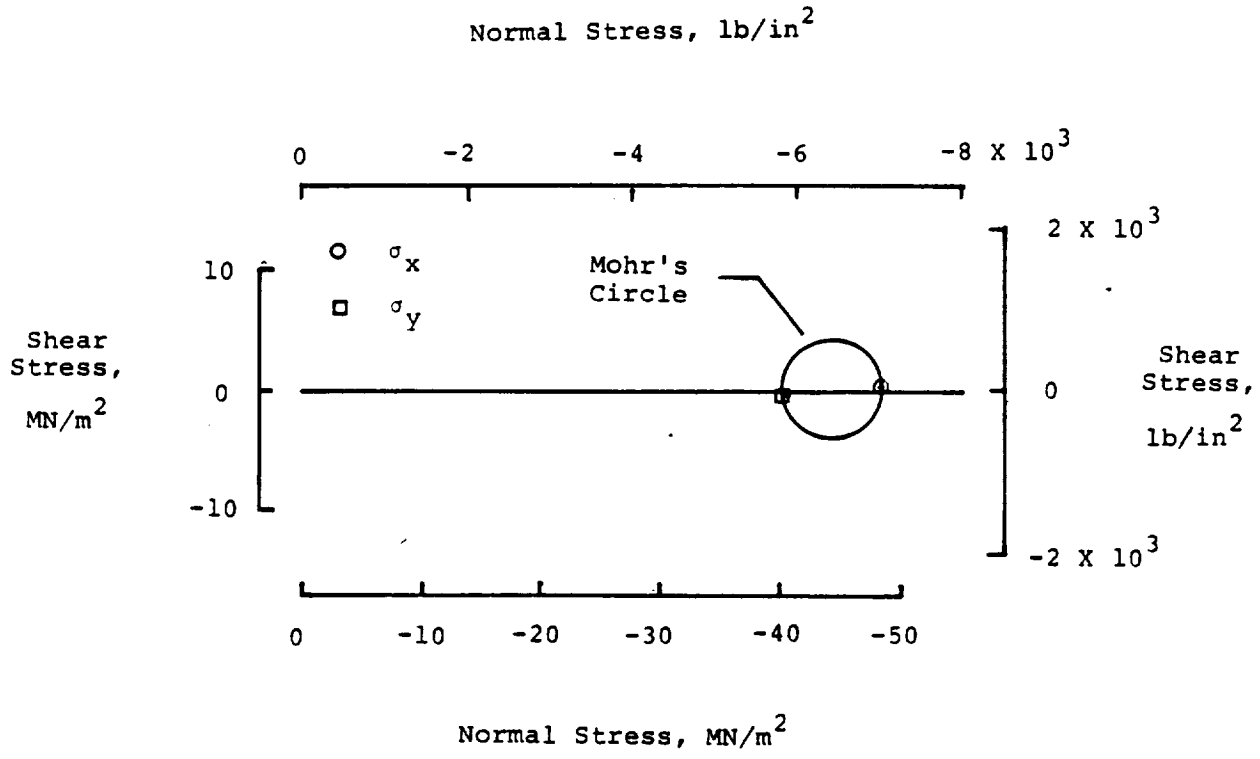

Figure 17. Mohr's Circle of stress for a typical state of skin thermal stress.

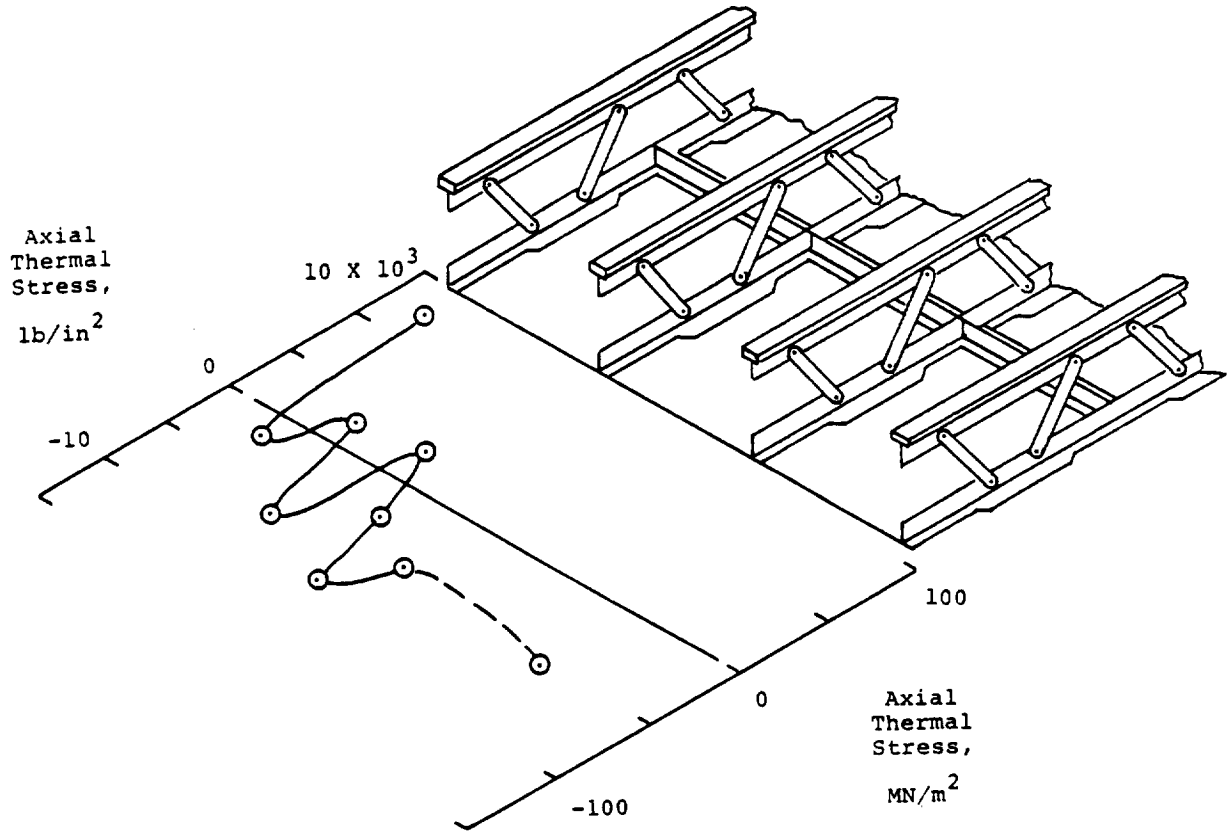

(a) Frame A.

Figure 18. Distribution of axial thermal stress across the skin of the specimen at time equals three minutes.

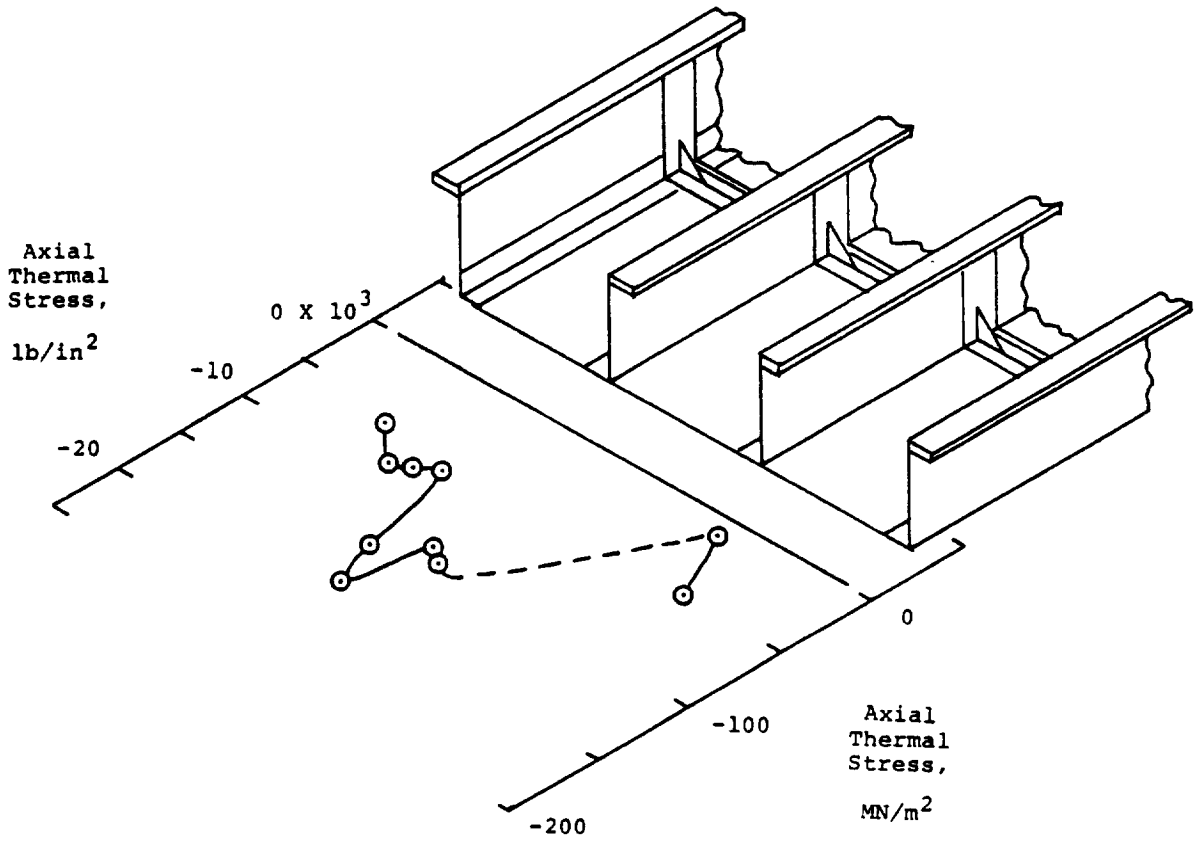

(b) Frame B.

Figure 18. Continued.

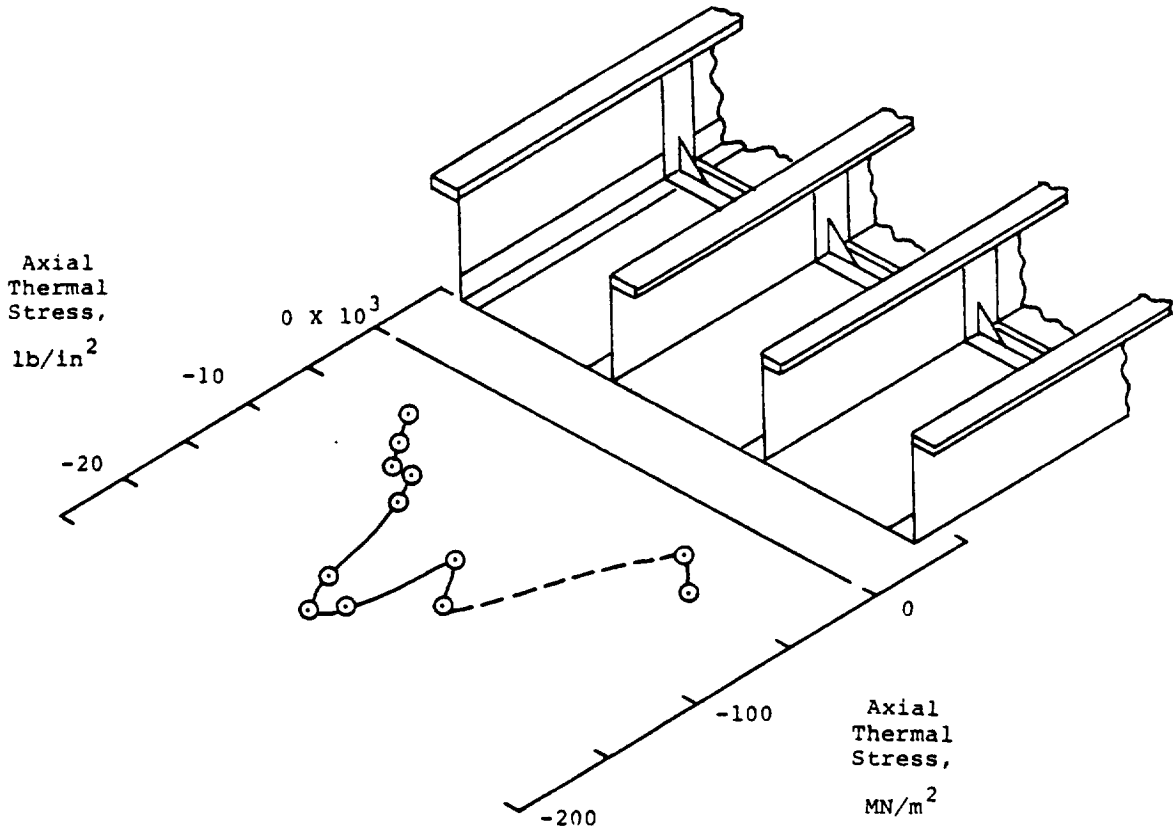

(c) Frame C.

Figure 18. Concluded.

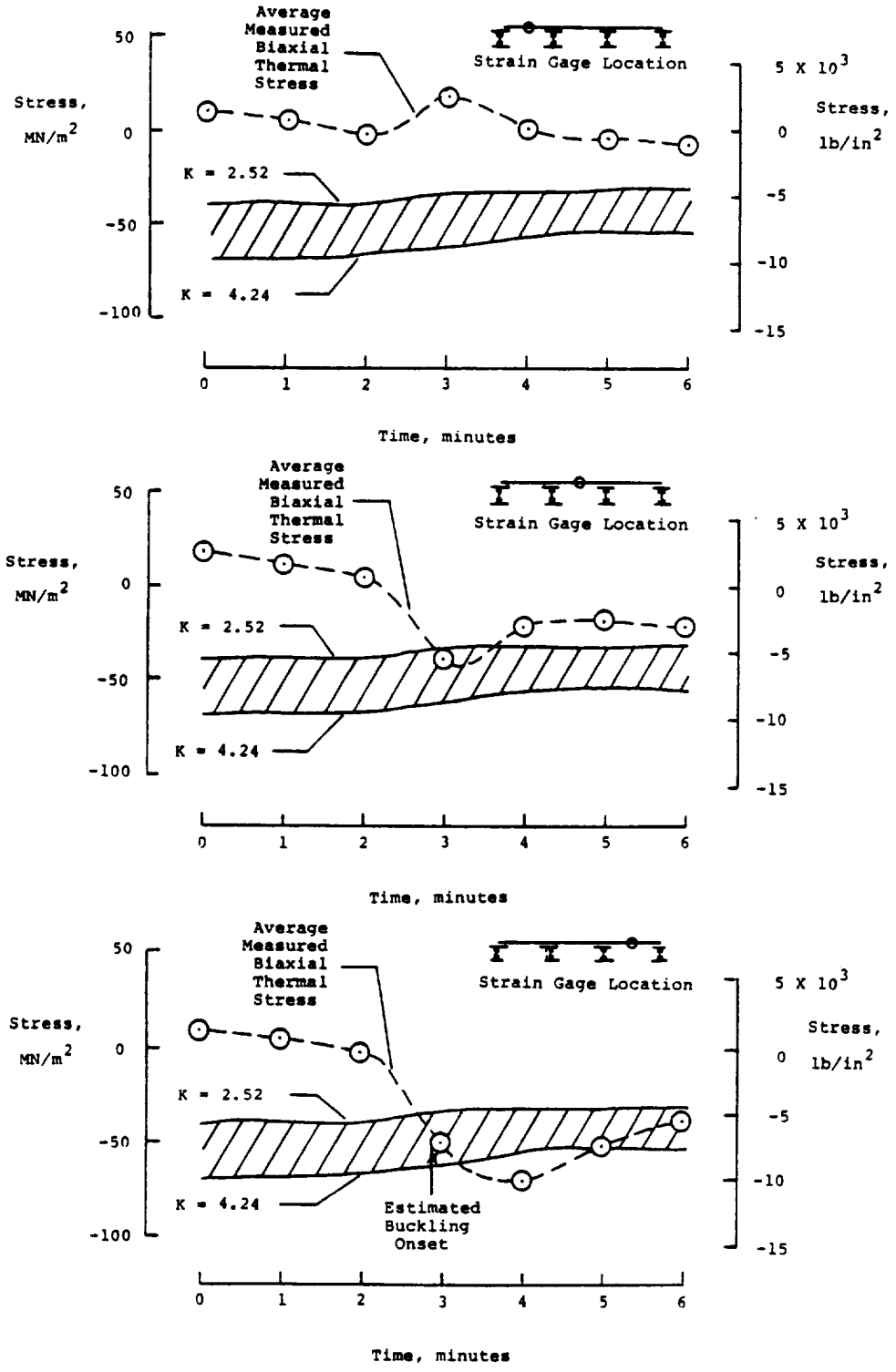

(a) Frame A.

Figure 19. Time history of axial skin thermal stress compared to estimated panel buckling strength.

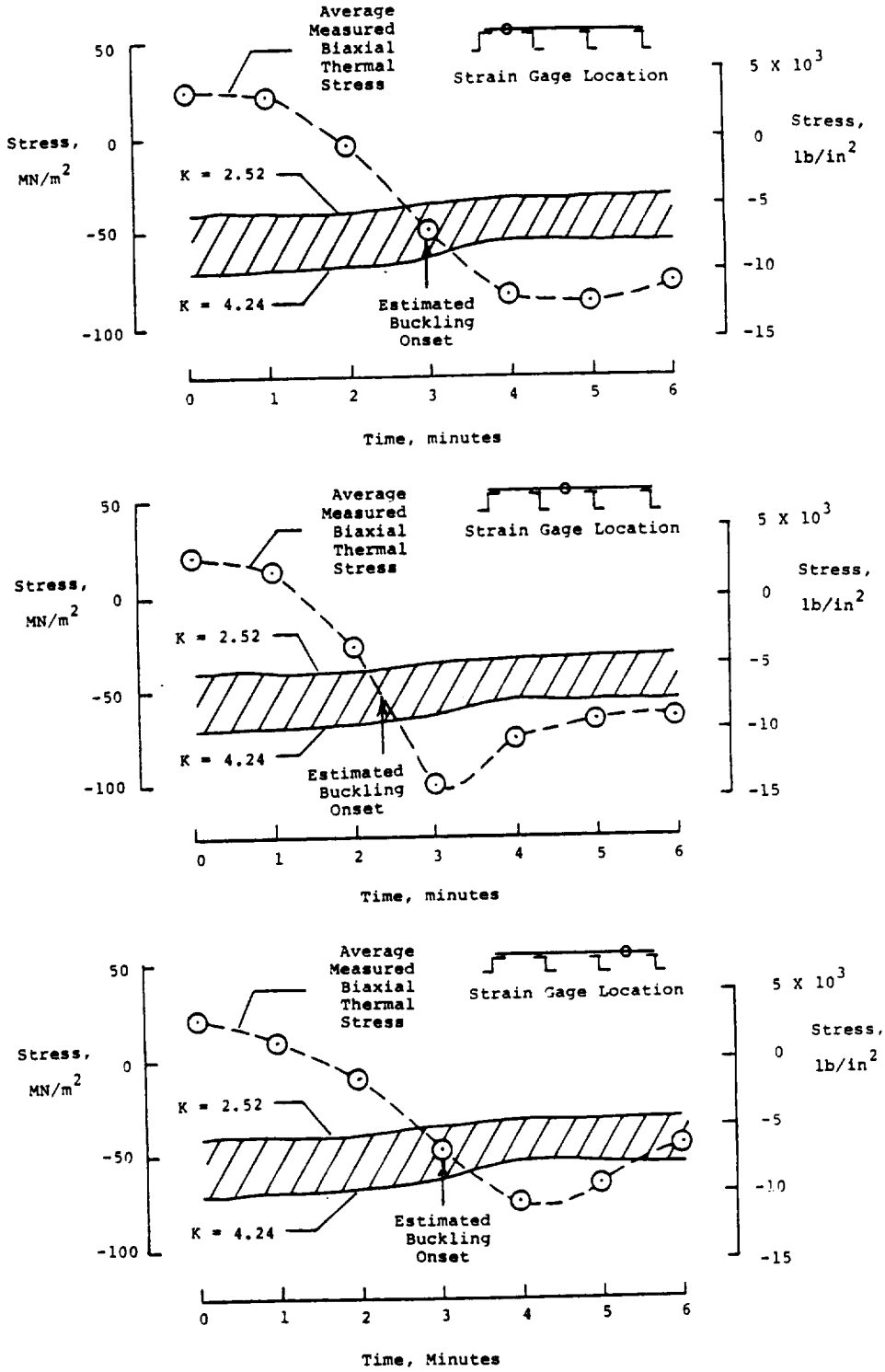

(b) Frame B.

Figure 19. Continued.

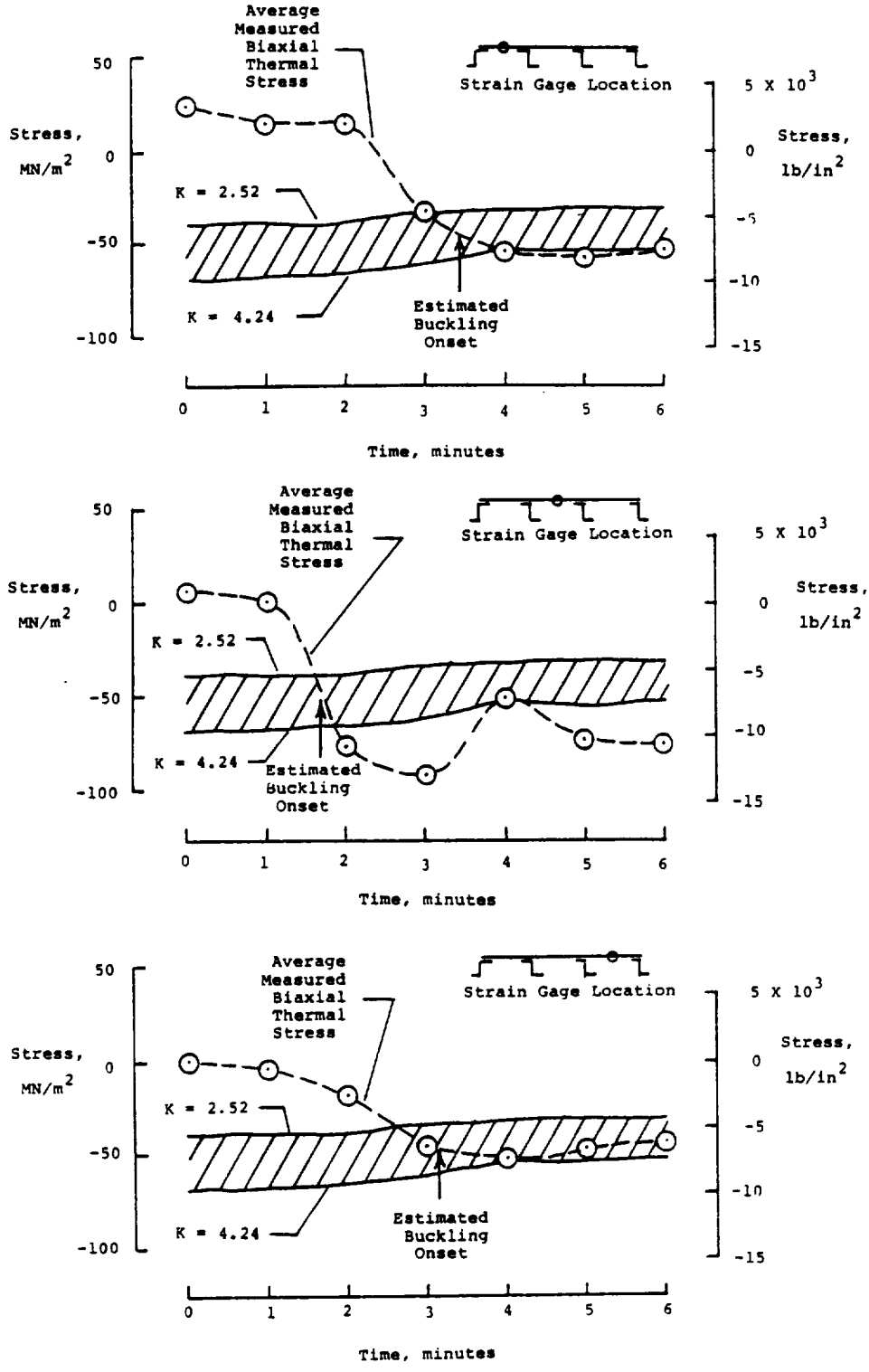

(c) Frame C.

Figure 19. Concluded.

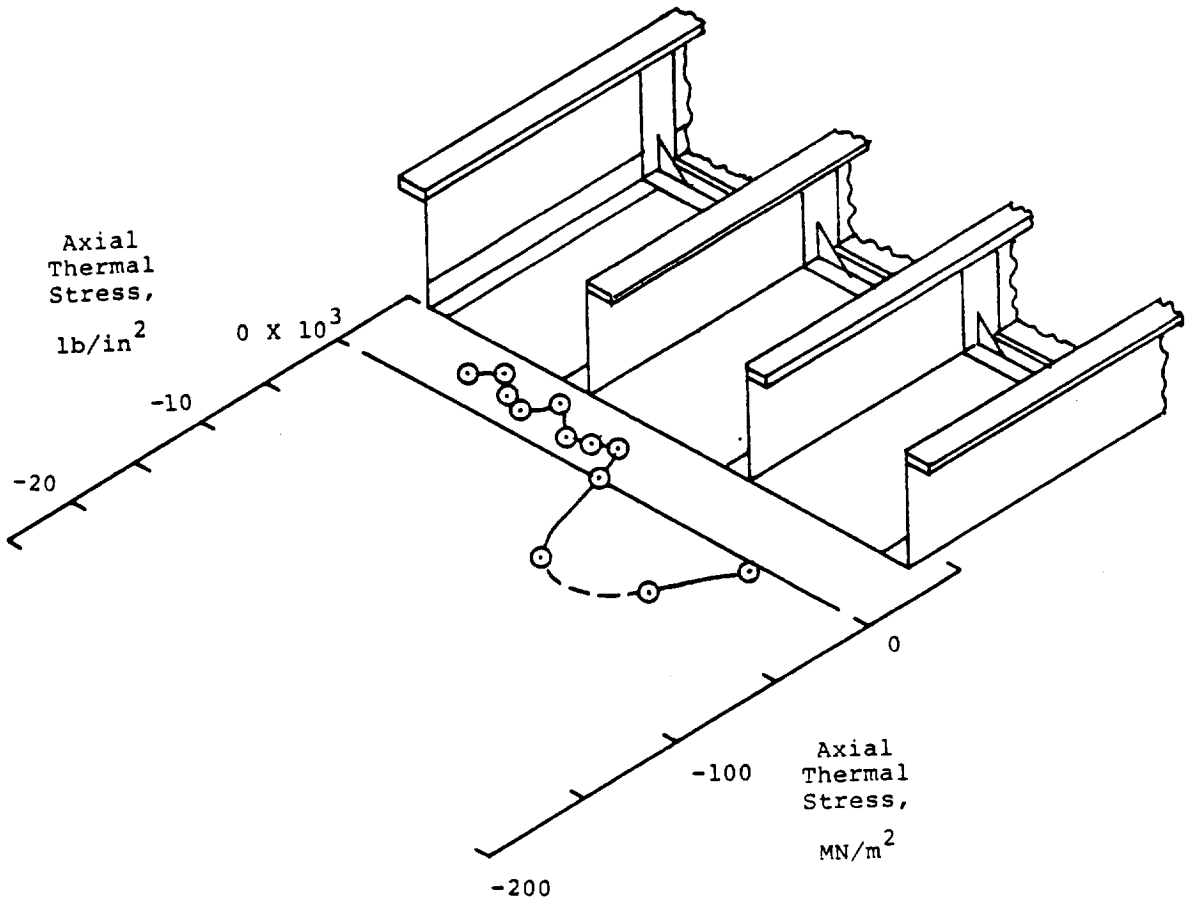

(a) Time = 1 minute.

Figure 20. Progression of axial skin thermal stress with time for Frame C.

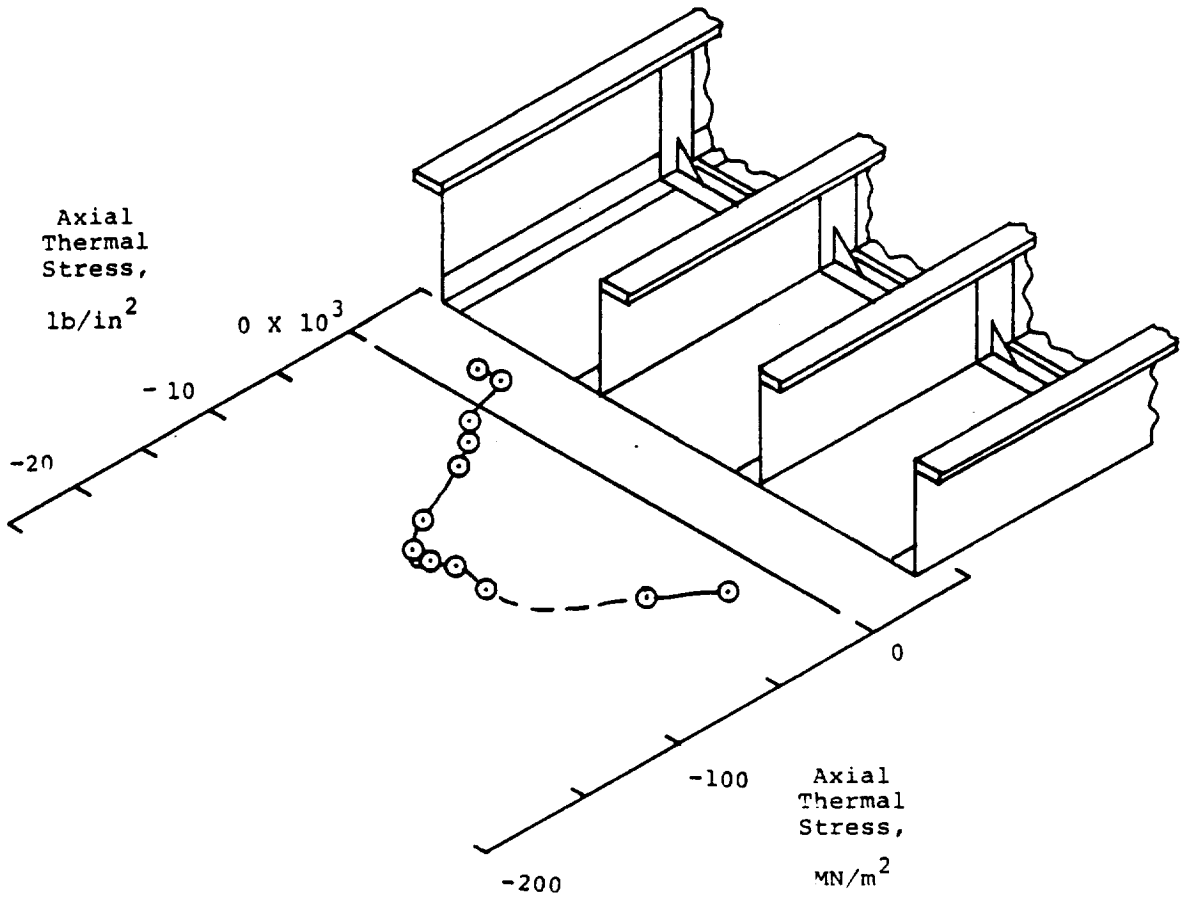

(b) Time = 2 minutes.

Figure 20. Continued.

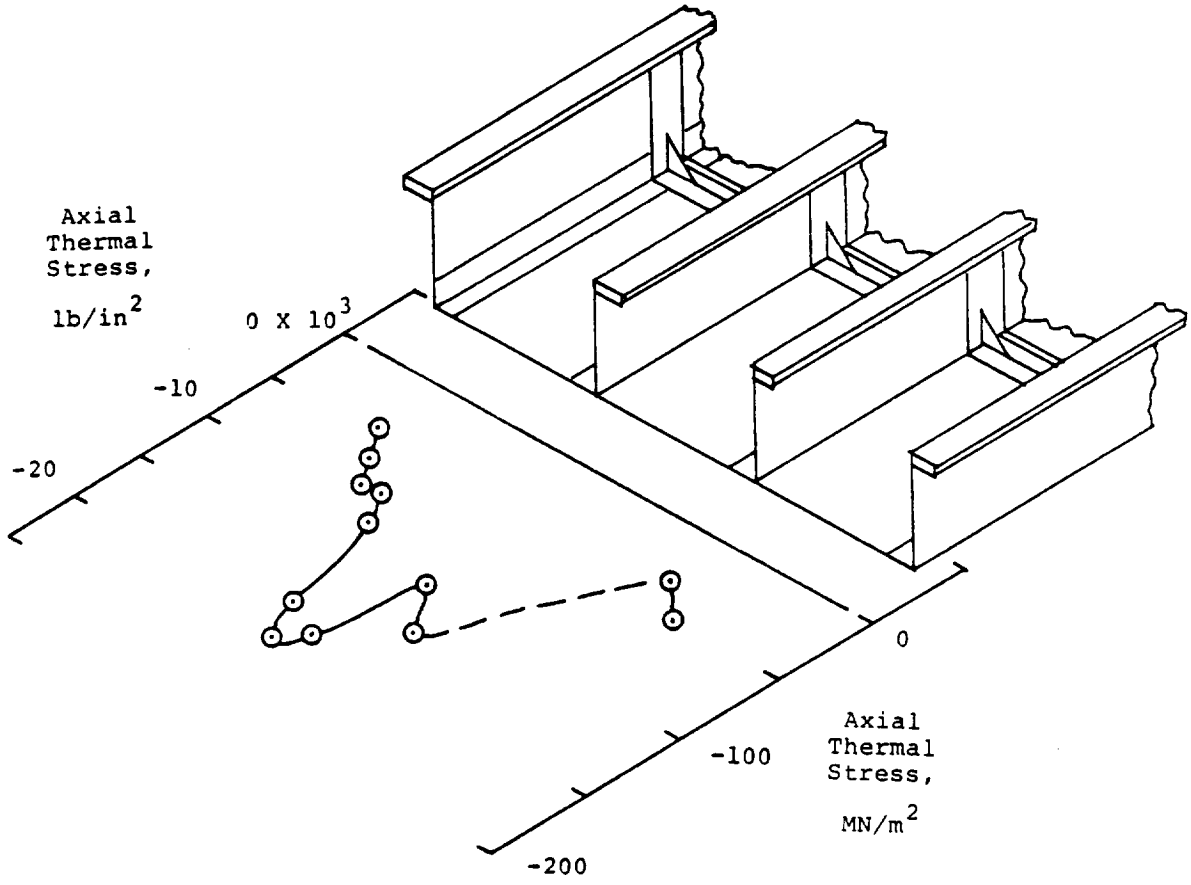

(c) Time = 3 minutes.

Figure 20. Continued.

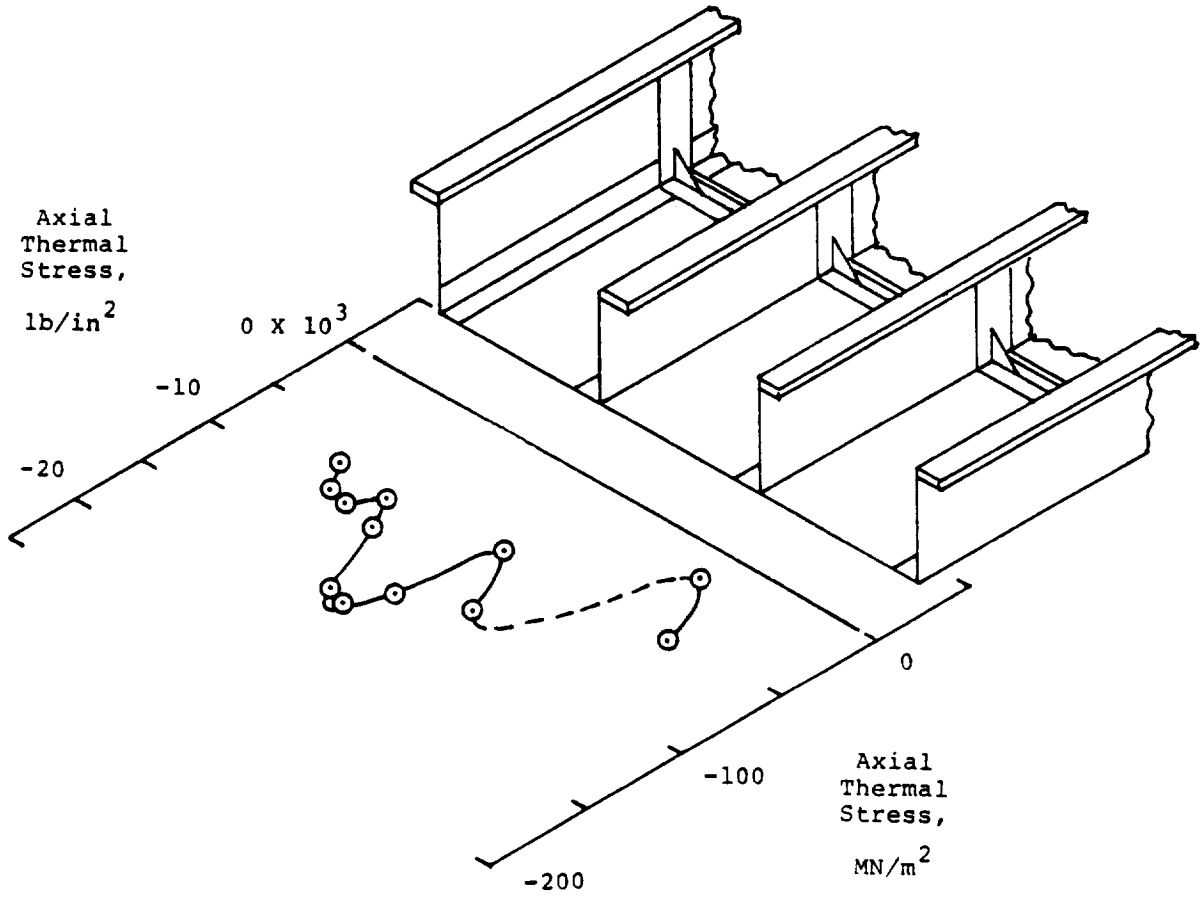

(d) Time = 4 minutes.

Figure 20. Concluded.

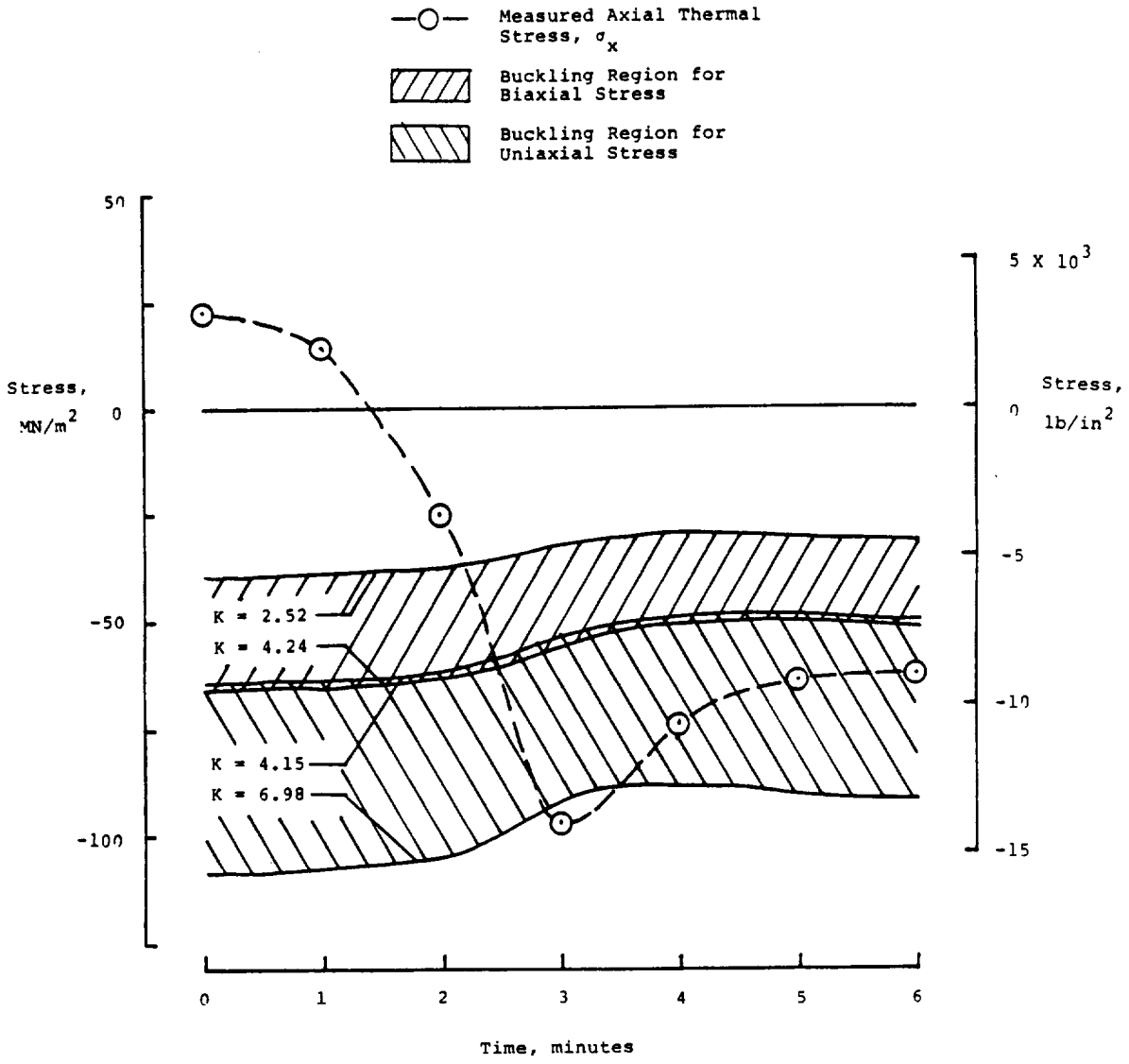

Figure 21. Time history of axial skin thermal stress compared to uniaxial and biaxial buckling strength.

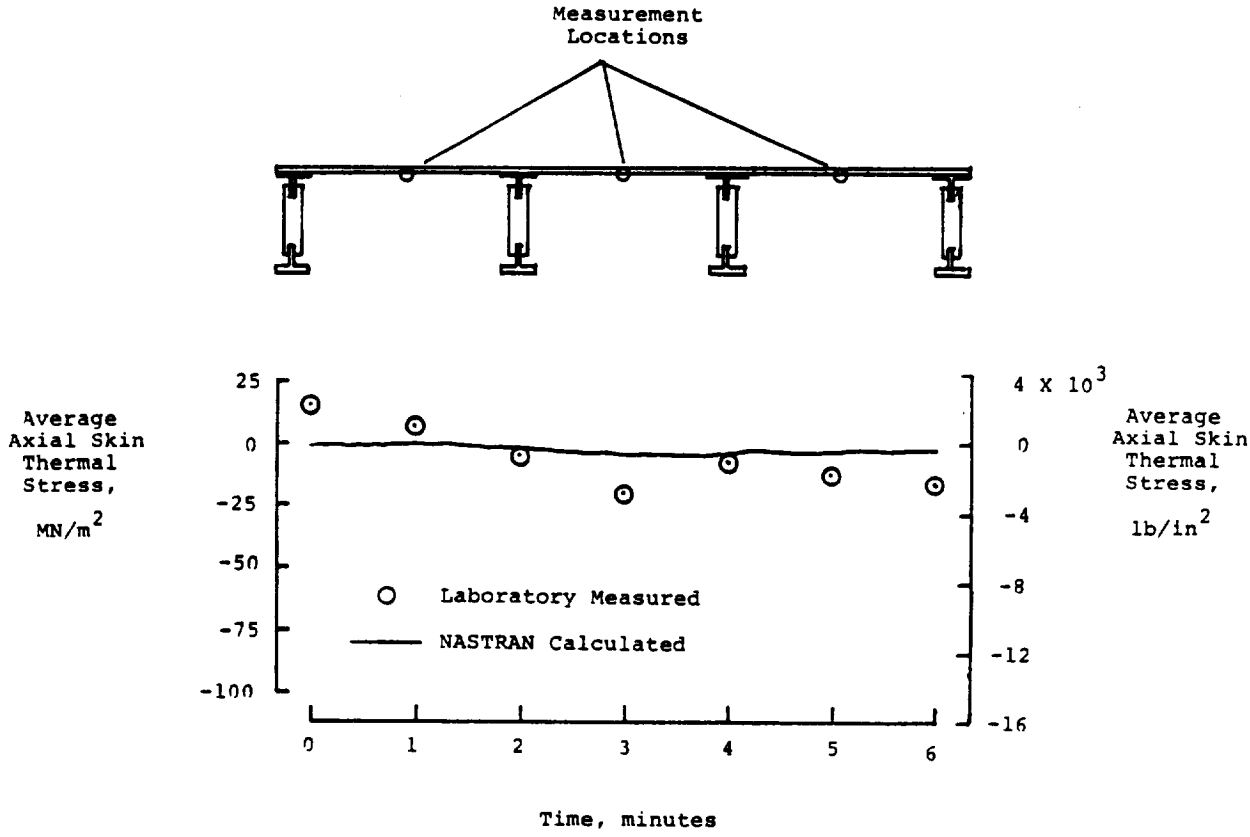

(a) Frame A.

Figure 22. Average center panel axial thermal stress compared with predicted values.

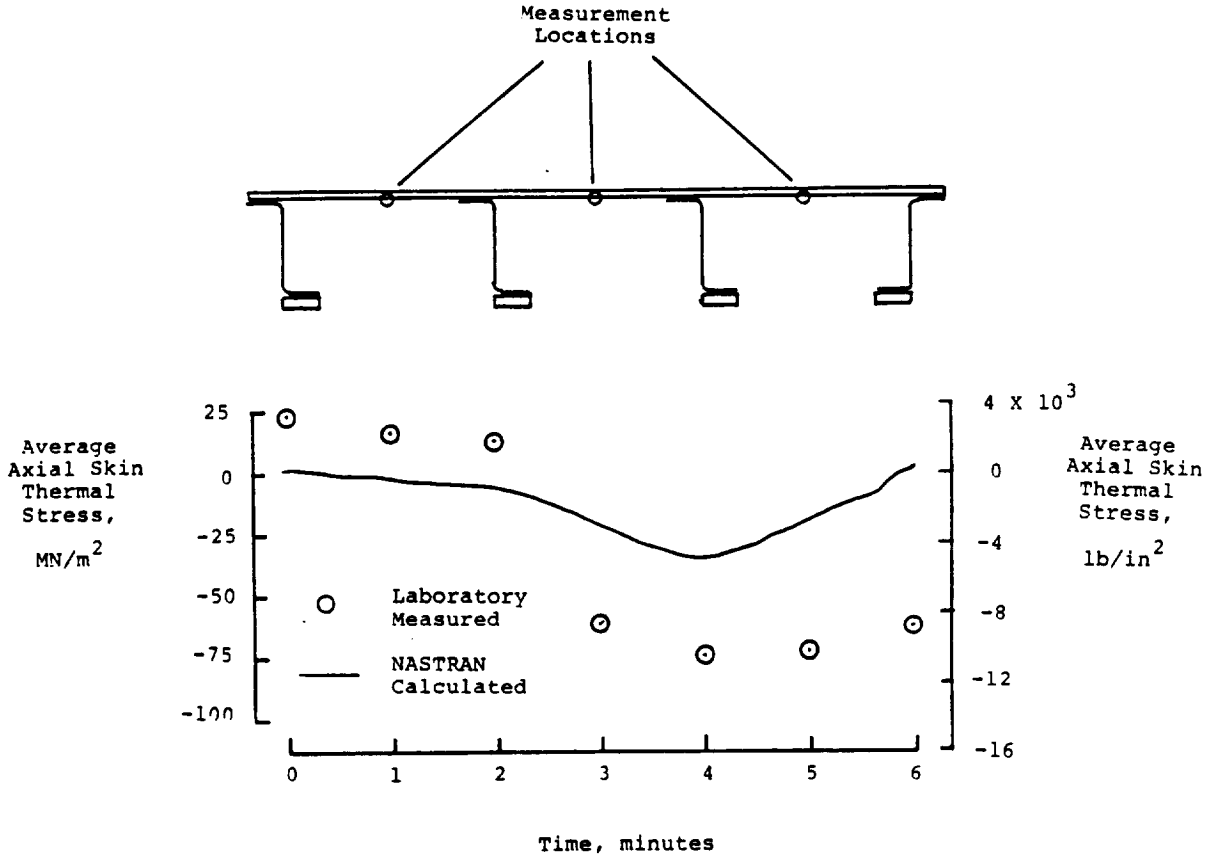

(b) Frame B.

Figure 22. Continued.

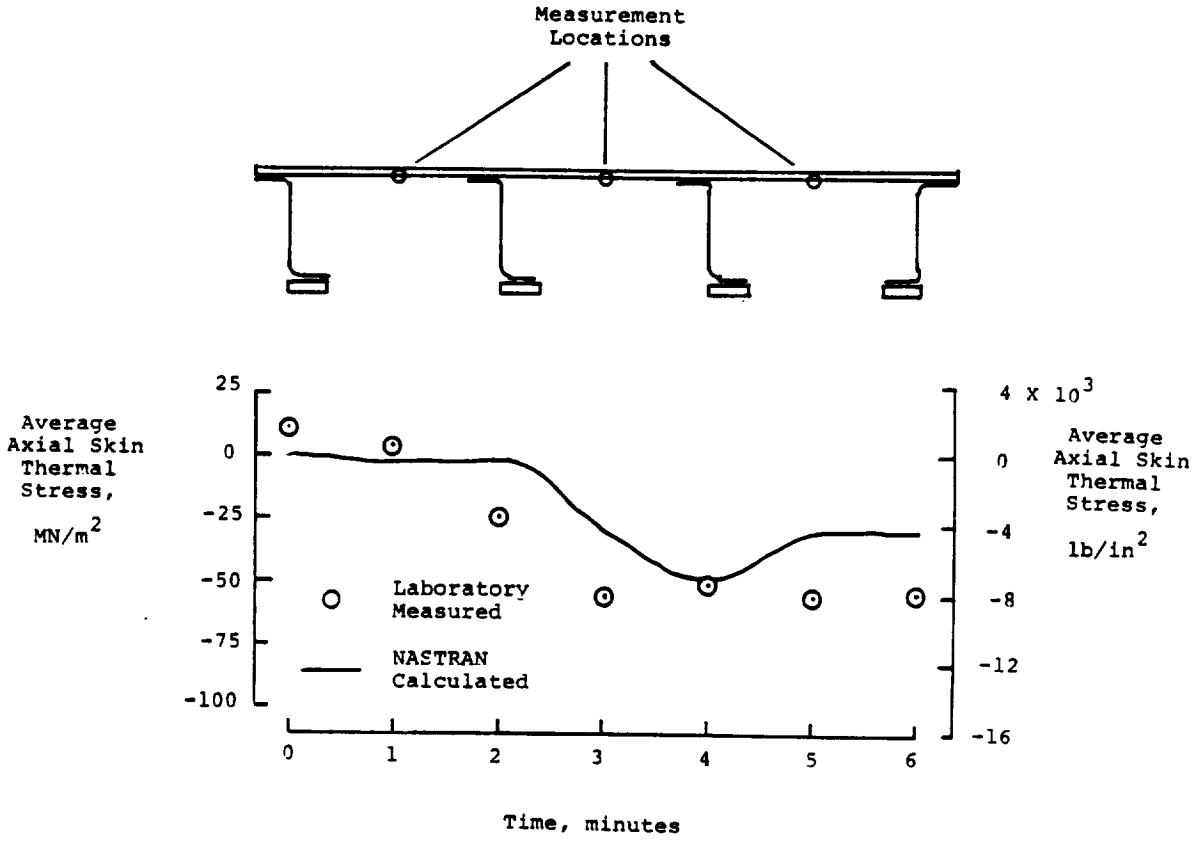

(c) Frame C.

Figure 22. Concluded.

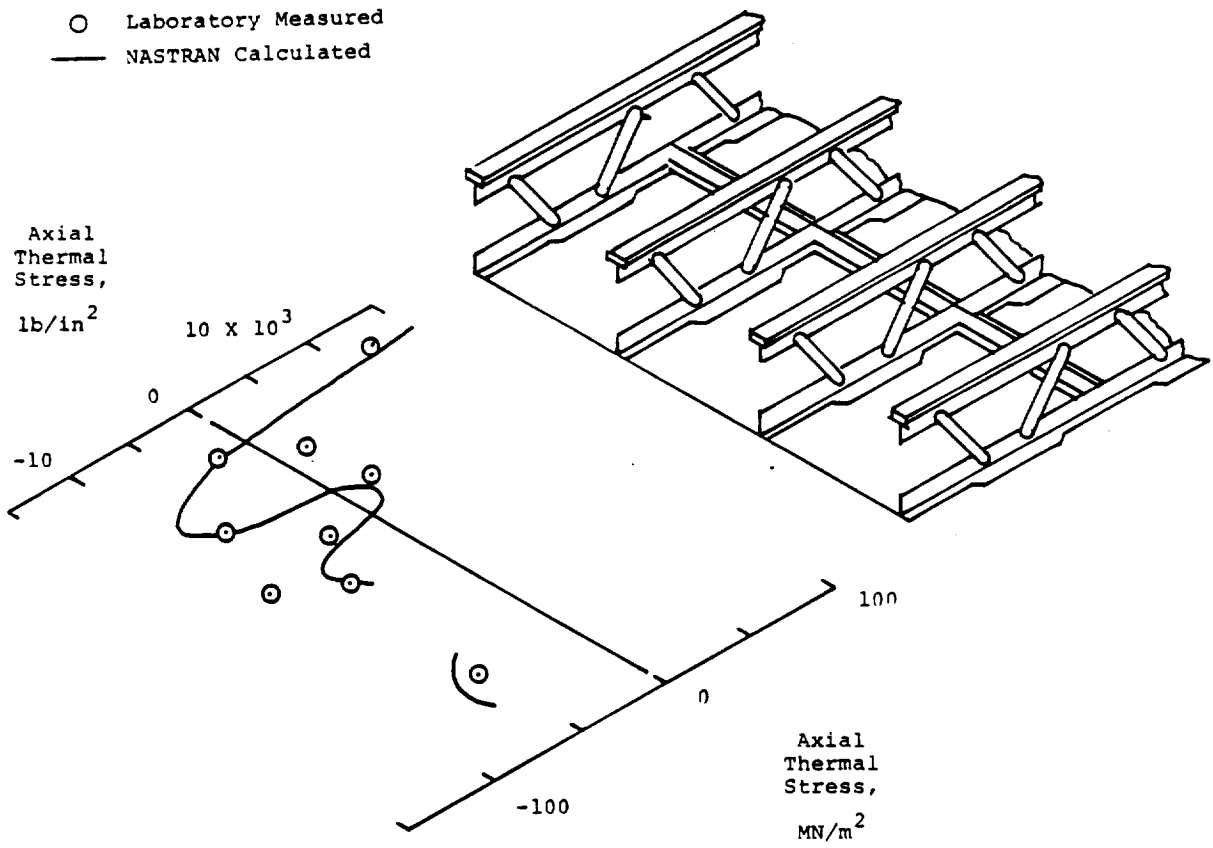

(a) Frame A.

Figure 23. Comparison of calculated and measured axial skin thermal stresses at time equals three minutes.

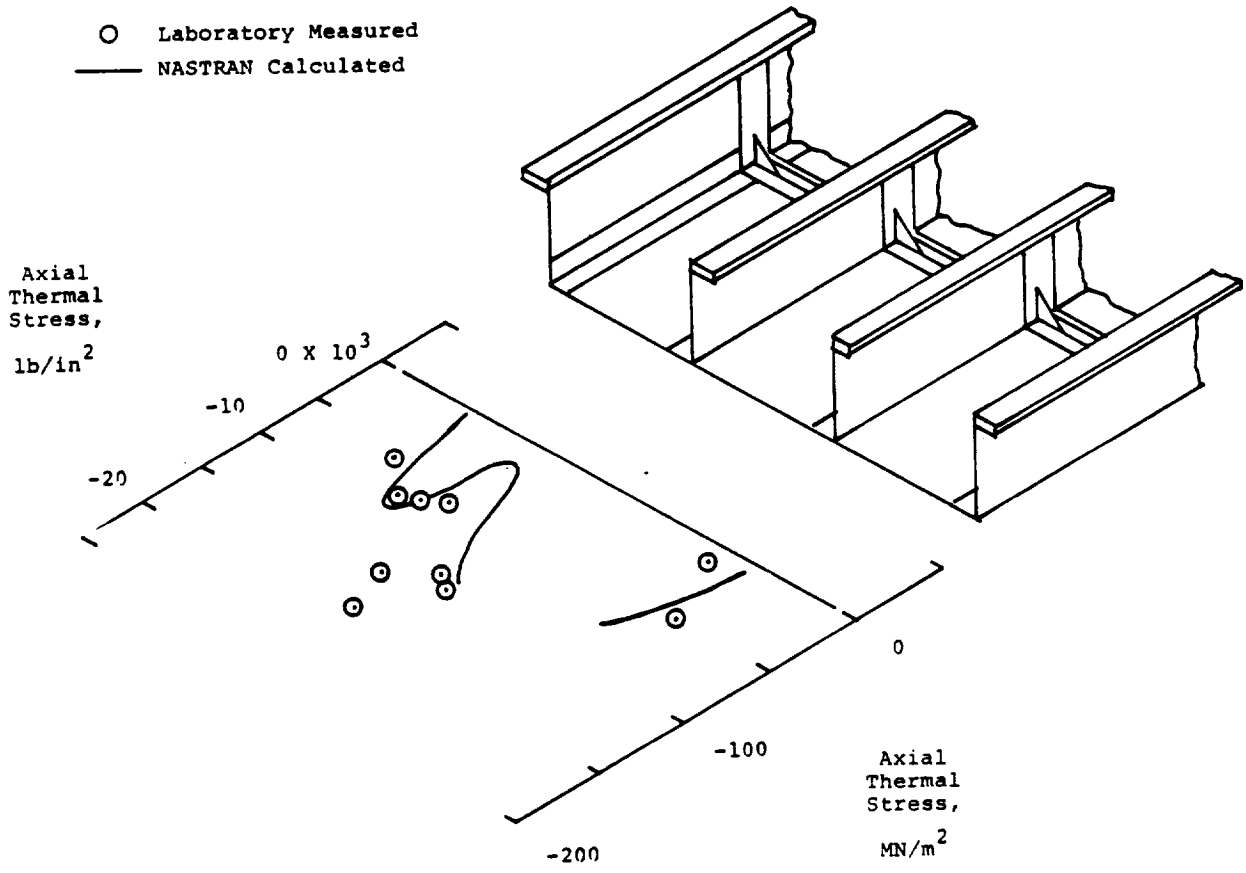

(b) Frame B.

Figure 23. Continued.

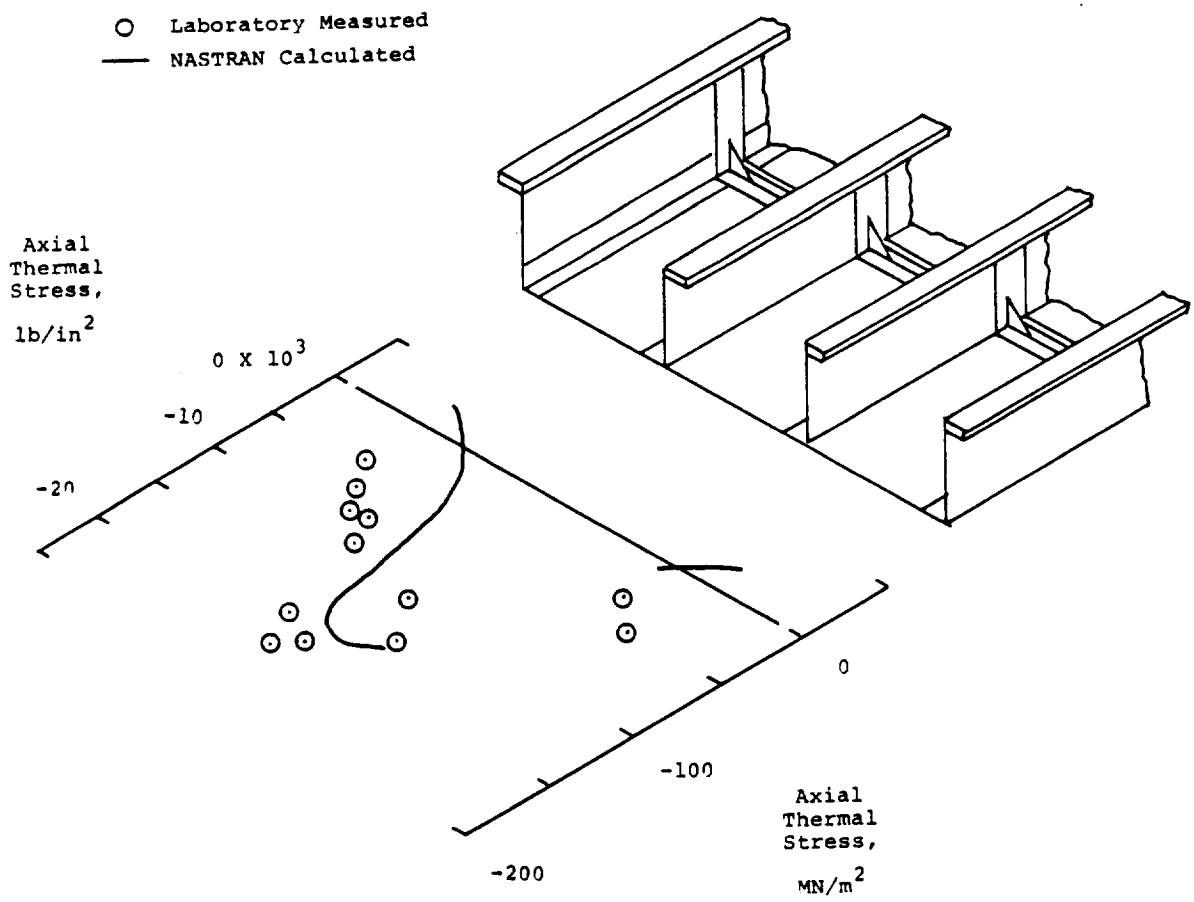

(c) Frame C.

Figure 23. Concluded.

1. Report No.	2. Government Accession No.	3. Recipient's Catalog No.
NASA TM-81352		

4. Title and Subtitle	5. Report Date
THE EFFECT OF THERMAL STRESSES ON THE INTEGRITY OF THREE BUILT-UP AIRCRAFT STRUCTURES	November 1980
	6. Performing Organization Code
7. Author(s)	8. Performing Organization Report No.
Jerald M. Jenkins	H-1138
	10. Work Unit No.
9. Performing Organization Name and Address	506-53-64
NASA Dryden Flight Research Center P.O. Box 273 Edwards, California 93523	11. Contract or Grant No.
	13. Type of Report and Period Covered
12. Sponsoring Agency Name and Address	Technical Memorandum
National Aeronautics and Space Administration Washington, D.C. 20546	14. Sponsoring Agency Code

15. Supplementary Notes

16. Abstract

Laboratory heating tests simulating a Mach 6 flight were conducted on three frame/skin specimens: (1) a titanium truss frame with a Lockalloy skin, (2) a stainless steel Z-frame with a Lockalloy skin, and (3) a titanium Z-frame with a Lockalloy skin. Thermal stresses and temperatures were measured on these three laboratory specimens for the purpose of examining their efficiency, performance, and integrity. Measured thermal stresses are examined with respect to material yield strengths, buckling criteria, structural weight, and geometric locations. Principal thermal stresses are presented and studied from the point of view of uniaxial and biaxial stress assumptions. Measured thermal stresses are compared to predicted values.

17. Key Words (Suggested by Author(s))	18. Distribution Statement
Thermal stresses Hypersonic structures Thermal buckling	Unclassified—Unlimited Distribution category: 05

19. Security Classif. (of this report)	20. Security Classif. (of this page)	21. No. of Pages	22. Price*
Unclassified	Unclassified	60	A04

For sale by the National Technical Information Service, Springfield, Virginia 22161